USE OF THE CEPSTRUM FOR PROCESSING MULTIPATH SIGNALS. II

Harry Schwarzlander, et al

Rome Air Development Center
Griffiss Air Force Base, New York

May 1975

192112

RADC-TR-75-117
In-house Report
May 1975

USE OF THE CEPSTRUM FOR PROCESSING MULTIPATH SIGNALS - II

Dr. Harry Schwarzlander
Dr. Bernard Silverman
Reinhard Hohensee

Post-doctoral Program

Approved for Public Release. Distribution Unlimited

Laboratory Directors' Fund

UNCLASSIFIED

SECURITY CLASSIFICATION OF THIS PAGE (When Data Entered)

REPORT DOCUMENTATION PAGE		READ INSTRUCTIONS BEFORE COMPLETING FORM
1. REPORT NUMBER RADC-TR-75-117	2. GOVT ACCESSION NO.	3. RECIPIENT'S CATALOG NUMBER AD-A011 669
4. TITLE (and Subtitle) Use of the Cepstrum for Processing Multipath Signals - II		5. TYPE OF REPORT & PERIOD COVERED Final Sept 70 to Dec 74
		6. PERFORMING ORG. REPORT NUMBER N/A
7. AUTHOR(s) Dr. Harry Schwarzlander Dr. Bernard Silverman Reinhard Hohensee		8. CONTRACT OR GRANT NUMBER(s) In-house
9. PERFORMING ORGANIZATION NAME AND ADDRESS Rome Air Development Center (DCLD) Griffiss AFB, NY 13441		10. PROGRAM ELEMENT, PROJECT, TASK AREA & WORK UNIT NUMBERS PE: 61101F Proj: 0171 Task: 72 WU: 01717208
11. CONTROLLING OFFICE NAME AND ADDRESS Same		12. REPORT DATE May 1975
		13. NUMBER OF PAGES ~~75~~ 80
14. MONITORING AGENCY NAME & ADDRESS(if different from Controlling Office) Same		15. SECURITY CLASS. (of this report) Unclassified
		15a. DECLASSIFICATION/DOWNGRADING SCHEDULE N/A

16. DISTRIBUTION STATEMENT (of this Report)

Approved for Public Release. Distribution Unlimited.

17. DISTRIBUTION STATEMENT (of the abstract entered in Block 20, if different from Report)

Same

18. SUPPLEMENTARY NOTES

RADC Project Engineer: Brian M. Hendrickson (DCLD)

This program was funded by the Laboratory Directors' Fund.

19. KEY WORDS (Continue on reverse side if necessary and identify by block number)

Data Transmission
Multipath
Signal Processing

20. ABSTRACT (Continue on reverse side if necessary and identify by block number)

This report summarizes an investigation into the use of cepstrum analysis in connection with the processing of communication signals which have been corrupted by multipath effects. Following up on an earlier phase of work, the primary objective consisted of the development and performance evaluation of an experimental setup, incorporating a minicomputer, for on-line cepstrum analysis of baseband communication signals. The purpose of the cepstrum analysis is the extraction of multipath information which can then be used to

DD FORM 1 JAN 73 1473 EDITION OF 1 NOV 65 IS OBSOLETE UNCLASSIFIED

SECURITY CLASSIFICATION OF THIS PAGE (When Data Entered)

20. (Continued)

maintain a multipath cancellation filter in correct adjustment. Another objective was the design of signal waveforms whose cepstra have desirable properties for this type of processing.

The basic experimental setup was completed and is described in this report. Test data is presented which was obtained with signals from various modems and with simulated simple discrete multipath interference. Various sources of error are discussed and analyzed. Several additional factors are considered which must be taken into account in implementing a practical system. The signal design work was also carried out and the principal concepts are summarized in the report.

TABLE OF CONTENTS

LIST OF ILLUSTRATIONS

LIST OF SYMBOLS

$\mathcal{C}_x(t')$	inverse Fourier transform of $\mathcal{L}_x(f)$; the complex cepstrum of x(t).
$\{c_x(k)\}$	complex cepstrum of a sampled signal sequence $\{x_k\}$.
$\{\overline{c_x(k)}\}$	mean cepstrum.
$\hat{c}(k)$	the largest magnitude cepstrum component.
$\{d_x(n)\}$	discrete Fourier transform (DFT) of sampled signal $\{x_k\}$, k = 0,1,2 ... (N-1).
DFT	Discrete Fourier transform.
FFT	Fast Fourier transform.
$\mathcal{F}_x(f)$	Fourier transform of the function x(t).
$f_s = T/N$	the sampling frequency at which incoming signal is sampled to allow cepstrum analysis.
$\hat{i}$	sample point corresponding to the position of largest cepstrum peak; i.e., $\underset{\sim}{\tau} = \hat{i}/f_s$.
J	uniformly distributed random variable which characterizes the sampling jitter introduced in the signal processing.
$\hat{j}$	stored intermediate calculation used in estimating τ.
$\mathcal{L}_x(f)$	cln $\mathcal{F}_x(f)$ = complex logarithm of $\mathcal{F}_x(f)$; logarithmic spectrum of x(t).
$\{\ell_x(n)\}$	discrete logarithmic spectrum of $\{x_k\}$.
N	total number of samples in a sequence.
P_m	probability of missing multipath spike, given that multipath is present, using threshold detection and cepstrum analysis.
P_{fa}	probability of false alarm; i.e., detecting a multipath spike when no multipath is present.
P_w	probability of incorrect detection; i.e., detecting a multipath spike at the wrong position in the cepstrum when multipath is present.
$\{q_i\}$	data sequence generated after threshold detection.

r	determines time of delay of delayed component of multipath signal, where $\tau = rT/N$.
T	period of periodic signal.
$w(k)$	discrete values of raised-cosine data window used in processing signal data.
$w(t)$	$= v(t) + \alpha v(t - \tau)$; distorted SSB signal.
$x(t)$	undistorted signal.
$x'(t_o)$	$\left.\frac{dx}{dt}\right\|_{t=t_o}$
$\check{x}(t)$	Hilbert transform of $x(t)$.
$y(t)$	multipath-distorted signal at baseband
$\overset{o}{y}$	complex envelope of $w(t)$, the distorted SSB signal.
α	attenuated amplitude of delayed portion of multipath signal; i.e., $y(t) = x(t) + \alpha x(t - \tau)$.
$\underset{\sim}{\alpha}$	an estimate of α.
β	attenuated amplitude of second delayed portion of signal when three transmission paths are present; i.e., $y(t) = x(t) + \alpha x(t - \tau_1) + \beta x(t - \tau_2)$.
δ_r	error introduced in the calculation of multipath spike, $c_m(r)$, caused by non-cyclic nature of multipath distortion.
Δ	peak-to-peak value of the sampling jitter.
ε_c	r.m.s. error per point in the cepstrum (averaged over the whole cepstrum).
ρ_i	ratio of r.m.s. noise to r.m.s. signal at the input (averaged over the input sequence).
$\{\theta_i^+\}$ and $\{\theta_i^-\}$	two stored threshold sequences used in the detection of the presence of multipath.
τ	time of delay of the delayed component of multipath signal; i.e. $y(t) = x(t) + \alpha x(t - \tau)$.
$\underset{\sim}{\tau}$	an estimate of τ.

1. INTRODUCTION

The work reported here is concerned with the use of the cepstrum for the reduction of multipath interference in communication systems. It is basically a continuation of work performed earlier and reported in [1]. The application toward which this effort is directed is HF data communication. Through the use of the cepstrum it should be possible, under suitable conditions, to extract at the receiver a good estimate of the pertinent multipath information on a continuing basis, without recourse to interspersing a special channel sounding signal with the normally transmitted communication signal. This multipath information could then be used to adjust a filter which is designed to cancel the multipath interference in the received signal.

The earlier work involved the development of suitable programs on a large computer - the GE 645 (now Honeywell 645) - and their evaluation using synthesized signal sample sequences. The results which were obtained looked promising. The present effort was therefore undertaken, with the aim of developing and evaluating on-line cepstrum computation using a small computer - the PDP-8. Such an arrangement allows the processing of actual modem signals that have been subjected to live or artificially imposed multipath distortion. It also differs from the earlier work by bringing into play the effects of very limited word length, the effects of sampling distortion, and lack of synchronization between the signal source, the multipath delay, and the sampling process.

The performance of such a cepstrum processing scheme depends to a certain extent on the waveshapes that are transmitted. Whereas the processor can be thought of as strictly supplementary to an existing communication system, the possibility of a complete system design, requiring the specification of optimum waveforms, was also considered.

For greatest ease of presentation, the main body of the report is rather brief and in summary form, while the technical details are presented in a number of appendices. The basic concepts of cepstrum analysis, and its use in processing multipath signals, are sketched in Section 2, and

Section 3 contains a brief review of the earlier work. The current effort and the results obtained are discussed in Section 4, with reference to the Appendices. The principal conclusions are listed in Section 5.

2. CEPSTRUM ANALYSIS APPLIED TO MULTIPATH SIGNALS

2.1 The Complex Cepstrum - Continuous Case.

A cepstrum of a signal x(t) is obtained upon applying the following sequence of generic operations:

Fourier transform - logarithm - inverse Fourier transform (2-1)

Interest in the cepstrum is due to the fact that if two signals $x_1(t)$, $x_2(t)$ are convolved in the time domain, then under suitable conditions the cepstrum of this convolution consists of the simple addition of the cepstra of the individual signals.

The detailed specification of (2-1) can take various forms, leading to different versions of cepstra. One such version has been called the "complex cepstrum" [4] because the complex logarithm is used in (2-1), although the cepstrum is actually a real function (if the signal is real). Given a signal x(t), then

its Fourier transform is $\mathcal{F}_x(f) = \int_{-\infty}^{\infty} x(t)e^{-j2\pi ft}dt$; (2-2a)

its logarithmic spectrum is $\mathcal{L}_x(f) = \text{cln}\,\mathcal{F}_x(f)$ (cln = complex logarithm); (2-2b)

its complex cepstrum is $\mathcal{C}_x(t') = \int_{-\infty}^{\infty} \mathcal{L}_x(f)e^{j2\pi ft'}df$. (2-2c)

The multi-valuedness of the complex logarithm is resolved by requiring continuity of $\mathcal{L}_x(f)$. The signal x(t) is recovered from $\mathcal{C}_x(t')$ by applying the sequence of operations F.T., exp., F.T.^{-1}.

Now suppose the signal x(t) is transmitted over a linear, time-invariant channel with impulse response h(t). The received signal is then y(t) = x(t)*h(t) and we have

$$\mathcal{F}_y(f) = \mathcal{F}_x(f)\,\mathcal{F}_h(f), \tag{2-3a}$$

$$\mathcal{L}_y(f) = \mathcal{L}_x(f) + \mathcal{L}_h(f) \tag{2-3b}$$

and also

$$\mathcal{C}_y(t') = \mathcal{C}_x(t') + \mathcal{C}_h(t') \tag{2-3c}$$

Thus, in both the logarithmic spectrum and the cepstrum, the contributions of the transmitted signal and of the channel add. If the impulse response h(t)

is impulsive, then so is $\mathcal{C}_h(t')$, so that the characteristics of the channel are most easily identified in the cepstrum domain (assuming that the signal cepstrum is not also impulsive).

Two different ways in which the cepstrum can be used to reduce multipath distortion are (a) "homomorphic filtering", and (b) channel identification coupled with a cancellation filter. In the first case, linear operations are applied in the cepstrum domain, in order to reduce - and possibly, eliminate altogether - the effect of $\mathcal{C}_h(t')$ in (2-3c). Transforming back to the time domain results in recovery of x(t) with little or no distortion due to the channel. In the other case, the pertinent channel parameters are estimated from $\mathcal{C}_y(t')$ and these estimates can then be used to adjust a multipath cancellation filter.

The simplest type of multipath channel is one which introduces a single discrete multipath component, with amplitude and delay that is approximately constant over an observation interval. The received signal y(t) is then

$$y(t) = x(t)*m(t) = x(t) + \alpha x(t - \tau), \tag{2-4}$$

where the multipath channel impulse response is $m(t) = \delta(t) + \alpha\delta(t - \tau)$. Applying (2-3) to the received signal (2-4) gives

$$\mathcal{F}_y(f) = \mathcal{F}_x(f)\ (1 + \alpha e^{-j2\pi f\tau});$$

$$\mathcal{L}_y(f) = \mathcal{L}_x(f) + c\ln(1 + \alpha e^{-j2\pi f\tau})$$

$$= \mathcal{L}_x(f) + \alpha e^{-j2\pi f\tau} - \frac{\alpha^2}{2} e^{-j4\pi f\tau} + \frac{\alpha^3}{3} e^{-j6\pi f\tau} - \ldots \text{ (for } a < 1);$$

$$\mathcal{C}_y(t') = \mathcal{C}_x(t') + \alpha\delta(t' - \tau) - \frac{\alpha^2}{2}\delta(t' - 2\tau) + \frac{\alpha^3}{3}\delta(t' - 3\tau) - \ldots \tag{2-5}$$

The effect of the multipath in the complex cepstrum is a sequence of impulses with spacing τ and weights determined by α. Therefore, if $\mathcal{C}_x(t')$ contains no impulses, the multipath parameters α and τ are easily identifiable in the cepstrum.

2.2 The Complex Cepstrum - Discrete Case

In practice, digital processing is employed. Given a sequence of N

samples $\{x_k\}$, $k = 0, 1, \ldots, N-1$, then its discrete Fourier transform (DFT) is

$$\{d_x(n)\} = \left\{ \frac{1}{N} \sum_{k=0}^{N-1} x_k e^{-j2\pi \frac{nk}{N}} \right\}, \quad n = 0, 1, \ldots, N-1;$$

its (discrete) log spectrum is $\{\ell_x(n)\} = \text{cln}\{d_x(n)\}$;

its (discrete) complex cepstrum is

$$\{c_x(k)\} = \left\{ \sum_{k=0}^{N-1} \ell_x(n) e^{j2\pi \frac{nk}{N}} \right\}, \quad k = 0, 1, \ldots, N-1.$$

The multi-valuedness of cln is, in general, not readily resolved in a unique manner in this case; however, this is of no concern at this point. Suppose $y(t)$ in (2-4) is sampled N times over $0 \leq t < T$, giving the sample sequence $\{y_k\}$, $k = 0, 1, \ldots, N-1$. Then $\{y_k\} = \{x_k\} + \alpha\{x_{k-r}\}$, where negative subscripts refer to samples taken prior to $t = 0$.

At this point, in order to simplify the discussion, the following idealized case will be assumed. Namely, assume that $\tau = rT/N$, where r is an integer, $|r| << N$. Also, assume $x(t)$ is periodic with period T, or at least $x(kT/N) = x((N + k)T/N)$ for $-r \leq k \leq -1$.

In this idealized case, transformation of the sequence $\{y_k\}$ gives

$$\{d_y(n)\} = \{d_x(n)(1 + \alpha e^{-j2\pi \frac{nr}{N}})\} \tag{2-6a}$$

$$\{\ell_y(n)\} = \{\ell_x(n)\} + \{\text{cln}(1 + \alpha e^{-j2\pi \frac{nr}{N}})\}$$

$$= \{\ell_x(n)\} + \{\alpha e^{-j2\pi \frac{nr}{N}} - \frac{\alpha^2}{2} e^{-j4\pi \frac{nr}{N}} + \ldots\} \tag{2-6b}$$

$$\{c_y(k)\} = \{c_x(k)\} + \{c_m(k)\}; \tag{2-6c}$$

where $\{c_m(k)\}$ is the cepstrum of the multipath channel response,

$$c_m(k) = \begin{cases} -\frac{N(-\alpha)^p}{p}, & \text{for } k = pr \bmod N \ (p = 1, 2, \ldots) \\ 0, & \text{otherwise} \end{cases} \tag{2-7}$$

Thus, for the idealized case, the discrete cepstrum (2-6), (2-7), exhibits the same features as (2-5) for the continuous case (Fig. 1). The impulses

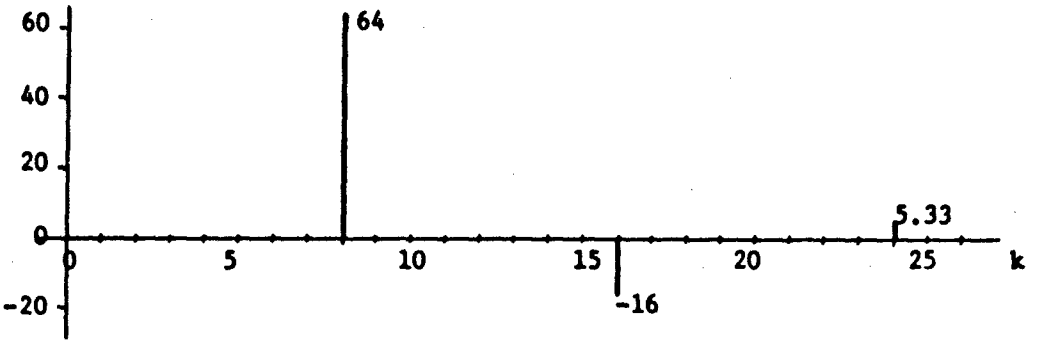

Fig. 1. Portion of Discrete Multipath Cepstrum, for N = 256, r = 8, α = 0.5

in (2-5) have become "discrete impulses" in (2-7). (The effect of removing the idealizing assumptions is considered in Section 2.4.)

Extractability of multipath information from (2-6) no longer depends - as in (2-5) - on the absence of impulses in the cepstrum of the desired signal; rather, the variability of $\{c_x(k)\}$ must be small over that range of k in which the most significant component(s) of (2-7) are expected to fall. If this is the case, a good estimate of α and the value of r can be obtained. This allows an approximation of $\{c_m(k)\}$ to be subtracted from $\{c_y(k)\}$, leaving $\{c_x(k)\}$ with little distortion. Inversion of the cepstrum computation then yields $\{x_k\}$ with little distortion. Alternately the estimates of α and r can be used to adjust a multipath cancellation filter, in which case it would not be necessary to perform a cepstrum computation for every consecutive sequence of N signal samples.

2.3 The Real Cepstrum

It turns out that for typical communication baseband signals, the variability of $\{c_x(t)\}$ is not small compared to $\{c_m(k)\}$, so that a useful estimate of the multipath parameters α and τ is not obtainable from the complex cepstrum. However, excessive variability of $\{c_x(k)\}$ is only exhibited by the odd part of the sequence, which is obtained from the imaginary part of $\{\ell_x(n)\}$ (the phase spectrum). If the odd part of $\{c_y(k)\}$ is deleted, there

remains $\mathcal{E}v\{c_y(k)\}$, the even part, which is obtained from $\mathcal{R}e\{\ell_y(n)\}$ and is therefore called the "real cepstrum". From (2-7) it can be seen that the real cepstrum of the channel response, $\mathcal{E}v\{c_m(k)\}$, incorporates all the multipath information except the polarity of r.

For these reasons, only the computation of the <u>real</u> cepstrum has been implemented as part of the work described in this report. The notation of (2-6c) is, therefore used from here on to denote real cepstra, thus, $\{\ell_x(n)\} = \ln|\{d_x(n)\}|$, etc.

The ambiguity in the sign of r, resp. τ, which is inherent in a multipath estimate based solely on the real cepstrum is assumed resolvable by other means. The basic processing steps are therefore as shown in Fig. 2.

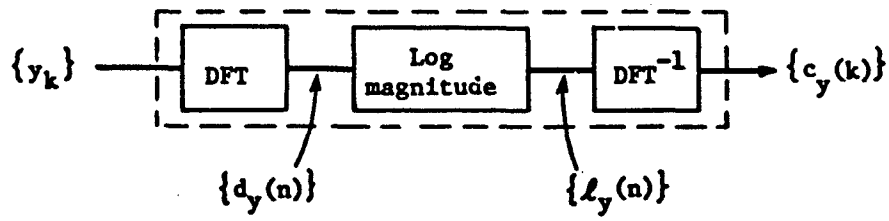

Fig. 2. Computation of the Real Cepstrum.

Since the real cepstrum does not carry the complete signal information, it cannot be used to reconstruct the undistorted signal. Therefore, the primary effort of this investigation has been to evaluate the extractability of the multipath parameters (α and τ) from the real cepstrum of the received signal

$$\{c_y(k)\} = \{c_x(k)\} + \{c_m(k)\}. \qquad (2\text{-}8)$$

The following observations can be made with regard to the extraction of α and τ:

a) Since $\{c_y(k)\}$ is even, only the first N/2 cepstrum points need to be examined.

b) If the range of possible multipath delays τ is known, the relevant portion of $\{c_y(k)\}$ may be further reduced, since only the first spike (or the first two spikes) of $\{c_m(k)\}$ are generally sufficiently large to

contribute to detection.

c) $\{c_x(k)\}$ is a random sequence, since it depends upon the transmitted information. However, a mean cepstrum, $\{\overline{c_x(k)}\}$, for a given type of transmission, can be obtained from measurements and can be subtracted from $\{c_y(k)\}$. This leaves the various cepstrum points as approximately zero-mean random variables (except for the superimposed multipath cepstrum).

d) The first spike of the multipath pattern ($p = 1$ in (2-7)) is then identified by locating the largest magnitude cepstrum value within the relevant region (after subtraction of the mean cepstrum). Either a single spike can be used to estimate α (in which case, the value of the spike divided by N/2 is the estimate), or a composite estimate based on the first two spikes can be obtained. Only the first scheme has actually been implemented.

e) A detection threshold is needed which, although causing some cases of weak multipath to be missed, minimizes the chance of a false-alarm. Especially, the chance of combined occurrence of a miss and a false alarm (at an incorrect value of τ) should be minimized.

2.4 Arbitrary Signals

Departing now from the idealized assumptions introduced in Section 2.2, suppose first that $\tau \neq r(T/N)$; i.e., τ is not an integer number of sampling intervals. It can be shown [1] that in this case, $\{c_m(k)\}$ is approximately expressed by samples of sinc-functions centered at τ, 2τ, ... (Note: $\text{sinc } t \equiv (\sin \pi t)/\pi t$). Thus,

$$c_m(k) \cong \mathcal{E}v\left[-N \sum_{p=1}^{\infty} \frac{(-\alpha)^p}{p} \text{sinc}\left[p\tau \frac{N}{T} - k\right]_{\text{mod } N}\right] . \qquad (2\text{-}9)$$

In order to extract the multipath parameters, it is therefore necessary to interpolate on sinc-functions. The basic steps comprising the detection algorithm for extracting estimates $\hat{\alpha}$ and $\hat{\tau}$ from the largest multipath cepstrum spike are then as follows:

i) Over the relevant portion of the cepstrum (see item b above) subtract the mean cepstrum.

ii) Identify the largest cepstrum component that exceeds threshold. If none is found, a "no multipath" decision is reached. Otherwise:

iii) Determine whether one of the cepstrum points adjacent to the largest multipath component also exceeds threshold. If not, and $c(\hat{k})$ denotes the largest magnitude cepstrum component, then $\alpha = 2c(\hat{k})/N$; $\underset{\sim}{\tau} = \hat{k}T/N$. Otherwise:

iv) Interpolate between $c(\hat{k})$ and either $c(\hat{k}+1)$ or $c(\hat{k}-1)$, whichever is larger. Let $\phi = c_y(\hat{k} \pm 1)/[c_y(\hat{k}) + c_y(\hat{k} \pm 1)]$; then $\underset{\sim}{\alpha} = 2c_y(\hat{k})/(N \operatorname{sinc}\phi)$, and $\underset{\sim}{\tau} = (\hat{k} - 1 \pm \phi)T/N$.

Practical communication signals, of course, do not have the periodic property postulated as part of the "idealized case" in Sec. 2.2. If a received signal (2-4) is observed over a finite interval (0,T), it is therefore no longer of the form $x(t) + \alpha x(t - \tau)$. Only the portion of the signal $x(t)$ within $(0,T-\tau)$ appears delayed (Fig. 3). On the other hand, a portion of $x(t)$ outside the observation interval enters as a result of the delay τ into the slot $(0,\tau)$.

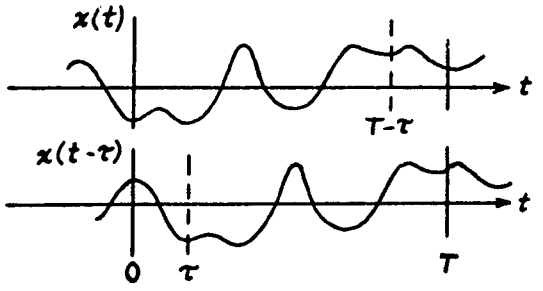

Fig. 3. A Signal and Its Delayed Version Within an Observation Interval.

The effect of this phenomenon on the cepstrum can be inferred in the following way. Writing

$$x_1(t) = \begin{cases} x(t), & 0 < t < T - \tau \\ 0, & \text{otherwise} \end{cases}$$

$$x_2(t) = \begin{cases} x(t), & T - \tau < t < T \\ 0, & \text{otherwise} \end{cases}$$

$$x_3(t) = \begin{cases} x(t) & -\tau < t < 0 \\ 0, & \text{otherwise,} \end{cases}$$

the follcwing expression is obtained for the received signal in (0,T):

$$y(t) = x_1(t) + \alpha x_1(t - \tau) + x_2(t) + \alpha x_3(t - \tau). \qquad (2\text{-}10)$$

Only $x_1(t)$ carries the multipath information (in the form of (2-4)). The remaining terms appearing in (2-10), $x_2(t) + \alpha x_3(t - \tau)$, can therefore be thought of as additive "noise" superimposed on the transmitted signal $x_1(t)$. Any additive noise in the time domain becomes combined non-linearly with the signal cepstrum to produce increased variability in the cepstrum, and it also depresses the magnitudes of the multipath spikes.

The latter effect can be understood by considering the effect of an additive disturbance $\varepsilon(t)$ in the DFT domain. At a frequency point n where $|d_x(n)(1 + \alpha e^{-j2\pi nr/N})|$ (the DFT for the "idealized case") is very small, addition of a small random vector $d_\varepsilon(n)$ is more likely to increase, rather than decrease, the magnitude of the DFT. This increase becomes magnified by the logarithm. Since the valleys of $\{|1 + \alpha e^{-j2\pi nr/N}|\}$ in general correspond to smaller values of $\{|d_x(n)(1 + \alpha e^{-j2\pi nr/N})|\}$ than the peaks, it can be seen that the additive component $\{d_\varepsilon(n)\}$ tends to lower the estimate of the multipath amplitude, $\underset{\sim}{\alpha}$.

Since this disturbance is introduced particularly at those frequency points where $d_y(n)$ is small, a choice of sampling rate is motivated which is not too high, so that the DFT domain does not cover an extensive frequency range containing little energy.

For a given sampling rate, the extent of the disturbance produced by these effects in the cepstrum is minimized if τ is as small as possible compared to N. This is one motivation for using a large N in computing the cepstrum. It has also been possible to considerably reduce this interference through the use of a data window with a $\sin^2$-rise ("Hanning") over the first and last few points of the sample sequence.

3. SUMMARY OF EARLIER WORK [1]

A computer study to assess feasibility of the processing scheme described above was carried out on the Honeywell 635 computer at RADC. For this purpose, various versions of cepstrum computation and multipath extraction programs were written and applied to synthetic signal sample sequences. The signal sample sequences, which were generated by computer, simulated the sampled output of a 16-channel HF modem in accordance with MIL-STD-188C. The output of such a modem consists of 16 frequency-division channels of 75 baud-per-second quadraphase PSK, with center frequencies equally spaced from 935 Hz to 2585 Hz. The computer-generated signal sequences simulated independent random modulation on all channels, and were based on various sampling rates, however, 8175 samples/sec was used for most tests. Sequences of 128, 256, 512, 1024, 2048, and 4096 samples were used (resulting in cepstra of the same lengths), but most of the work was done with 512 samples.

A single, discrete multipath component was introduced into the signal, usually with a delay equal to an integer number of sample spaces. However, delays of an odd number of half-sample spaces were also investigated, since at such values of delay the extractability of the multipath parameters from the cepstrum is poorest.

Initially, it was attempted to work with the complex cepstrum, thus leaving open the option of eliminating the multipath interference by filtering in the cepstrum domain ("homomorphic filtering"). It was found, however, as pointed out in Sec.2.3, that the random fluctuations in the complex signal cepstrum were so great as to mask the contribution of the channel. This problem could be overcome by working only with the real cepstrum. The undistorted signal cannot be reconstructed from the real cepstrum since the phase spectrum has been lost; but the multipath parameters can be estimated in the cepstrum (except for the polarity of τ, which must be determined by other means) so that the adjustment of a cancellation filter can be made to follow the running sequence of estimates obtained in this manner.

On the basis of the data obtained with 512-point sample sequences, with $\alpha = 0.2$ a multipath detection probability greater than 0.95 was estimated over a range of τ from about 1 ms to about 3.7 ms (see Fig. 2.2 of [1]). In

the vicinity of $\tau = 2$ ms., the estimates of α were within $\pm$ .07 with probability 0.95 (see Fig. 28 of [1]).

The steady-state signal-to-interference ratio at the output of an ideal cancellation filter was determined as a function of the error in the estimates of the multipath parameters. under the assumption of a time-invariant multipath characteristic. Values of 20 db signal-to-interference ratio were obtained with high probability over a wide range of α (see Figs. 27 and 28 of [1]).

The effect of varying the length of the original sequence used for cepstrum processing was also explored [6]. With the type of signal described above, it was found that the use of 128-point sequences resulted in excessive errors, but that useful results could be obtained by processing 256-point sequences.

All these results were obtained under idealized conditions as follows:

no additive noise was considered;

no timing jitter, sampling error, and other effects pertaining to the analog waveform and A/D conversion were considered;

only a single, discrete, fixed multipath component was considered;

negligible round-off error was introduced into the computations by the 635 computer.

4. THE CURRENT EFFORT

4.1 Objectives

The earlier work, summarized in the preceding section, indicated that considerable reduction in multipath distortion can be achieved with the aid of cepstrum processing. However, these results were obtained under very idealized conditions. The next phase of work, reported herein, was therefore initiated with the aim of developing and evaluating a test setup which would correspond more closely to a practical signal processor. Specifically, it was desired to process actual modem waveforms (inputs to a receiving modem). This objective can be divided into two stages:

a) modem waveforms are locally generated, with multipath distortion artificially introduced;

b) modem waveforms are demodulated test transmissions which have been sent over a long distance HF loop or other type of multipath channel.

Furthermore, in order to operate within the typical limitations of a practical special purpose digital processor which is dedicated to on-line cepstrum processing (e.g., small word size, small memory), the necessary processing operations were to be implemented on a small computer. The aim was to use the resulting test setup first on signals incorporating a single discrete multipath component in order to examine the extractability of multipath information via the cepstrum, for different types of modems. This could then be extended, depending on available time, to more complicated multipath structures, and to an examination of the effects of additive noise.

Because the usefulness of the cepstrum for extracting multipath information depends strongly on the nature of the signal, another phase of the current effort had the aim of identifying, or designing, types of waveforms which are best suited for such processing.

4.2 Accomplishments

4.2.1 On-Line Cepstrum Analysis

The development of a basic on-line cepstrum processing capability was completed, using a PDP-8I computer at DICEF*. The computer

*Digital Communication Experimental Facility, RADC.

programs, and the overall test setup are described in Appendix A. It turned out that a major part of the overall effort went into writing and debugging the PDP-8 programs. This was mainly because all programming was done in machine language, in order to minimize core storage requirements and thus to be able to accommodate all programs, and also provide adequate space for data, within the 4K core.

For these reasons, the debugging of the various routines was completed only near the end of the project period, so that there remained not much time to collect test data.

Problems with equipment also caused some delay. One of these was a control circuit failure in an incremental read-write magnetic tape unit which had been connected to the PDP-8I. Some time had been spent to program the PDP-8I to work with this tape deck, in order that programs could be loaded from tape, and data recorded on the tape. The tape deck had also been viewed as an augmentation of available storage capacity. Thus, additional programs (for instance, detection of two multipath components) could have been called into core when needed, and therefore would not require a permanent core allocation. However, the failure which occurred could not be corrected in time for the tape deck to be used on this project.

4.2.2 Test Results

The completed on-line cepstrum analysis and multipath parameter estimation system (as described in Appendix A) was operated with signals derived from three different data modems, as described in Appendix C. A test consisting of an extensive series of detection runs was made only with the Codex 9600 modem. However, the limited data which was obtained with the other two modems indicates that the Codex results can be taken as representative for the performance of all three types of modems. The data from this test is presented in Section C.2.1 and is analyzed in Appendix D. The test was conducted with the following multipath parameters:

$$\alpha = 0.5, \tau = 2.9 \text{ ms.}$$

The sampling rate was approximately 7000 samples/sec., which made the multipath delay approximately equal to 20.3 sample spacings.

The results of the Codex detection test were disappointing for two

reasons which will be discussed in turn, namely:

a) the wide spread in the estimate of α; and

b) the large number of detection errors.

The standard deviation for the set of α-estimates (using only those estimates which resulted from correct detections) is 0.102; furthermore, this value would be even larger (by about 10%) if a correction for multipath cepstrum depression had been applied to the data. In order to be able to estimate the contribution, to the variability of the α-estimates, of various errors introduced in processing, computations of these errors are carried out in Appendix D (based on the analysis of errors in Appendix B). It is shown there that the largest source of error is the timing jitter which was inadvertently introduced into the sampling process. Nevertheless, based on the approximations of Appendix B and Appendix D, a rather small estimate of the total processing error was obtained. As is pointed out in Sec. D.2, however, this estimate is very likely to be on the low side.

In summary, the data and analysis suggests that, although errors introduced in processing have produced a noticeable effect in the cepstrum, this effect does not account for the major part of the variability in α-estimates. It must therefore be concluded that a good part of the variability is inherent in the particular types of modem signals which were used.

Turning now to the large number of detection errors (25 out of a total of 201 multipath estimates), it is clear that the above comments apply here also. Both of the plots of signal cepstrum statistics (Figs. C1 and C7) imply a rather large variability of the signal cepstrum. The question as to the extent to which this is due to errors introduced in processing is again addressed by Appendix D. On the other hand, using the standard deviation of the (noisy) signal cepstrum, a computation discussed in Section D.1 yields a much smaller probability of wrong detection than actually obtained. Reasons for this discrepancy are listed in that Section. The question arises whether processing errors significantly affect the shape of the cepstrum distribution and in this way contribute disproportionately to the occurrence of detection errors. This has not been investigated.

4.2.3 Analysis of Other Factors Affecting Practical Application

The tests described in the preceding Section were of limited scope in a number of ways:

a) Only a single multipath component was used of fixed magnitude and delay.

b) The overall test was carried out strictly at baseband.

c) No actual multipath cancellation was performed.

The relatively simple algorithm, described in Sec. 2.4, for extracting the multipath parameters can no longer be used if the presence of more than one multipath component is anticipated. An algorithm applicable to the use of two multipath components, that is, a channel with the impulse response

$$h(t) = \delta(t) + \alpha\delta(t - \tau_1) + \beta\delta(t - \tau_2), \qquad (4\text{-}1)$$

is presented in Appendix E. From Section E.1 it is clear that multipath detection, and parameter estimation, under the assumption that two multipath components are present, is much more involved than in the case where only a single multipath component is assumed. Not only must several cepstrum peaks be taken into account (whose magnitudes are not necessarily linearly related to the multipath coefficients), but rather fine discrimination of their relative magnitudes may be required, as is evidenced by Fig. E1. This means that the results obtained with this algorithm are much more affected by signal cepstrum variability and additive noise than those obtained in the case of a single multipath component. Extraction of multipath parameters for even more complicated multipath structures appears to be out of the question, except in special cases. In such cases, multipath cancellation by homomorphic filtering may be possible, provided that an effective separation of signal cepstrum and multipath cepstrum can be arranged.

In Appendix G, the analysis was extended to HF signals, using SSB and DSB modulation. It is shown there (Eq. G-9) that ordinary SSB demodulation of a multipath signal results in a received baseband signal in which the multipath appears in a more complicated way, involving the Hilbert transform. Complex demodulation, on the other hand, gives the simple baseband signal (G-13) which, however, is complex. Due to the fact that the received multipath amplitude coefficient α' is then also complex, cepstrum analysis will

have to be applied to the complex signal rather than only its real part. Another factor to be considered is the fact that the argument of the coefficient α' is $-\omega_o\tau$ (Eq. G-14), where ω_o is the carrier angular frequency, so that it is very sensitive to small changes in τ. These observations indicate that some modifications of the present processing scheme are required in order to make it applicable to actual HF signals, even if only a single multipath component is assumed.

In order to assess the overall performance of a multipath processor, the performance of the actual cancellation scheme used must be taken into account. In [1], signal-to-interference ratio at the canceller output was plotted in Fig. 27 as function of α and $\underset{\sim}{\alpha}$, for the case of an ideal recursive cancellation filter operating in steady state, and without discrepancy between τ and $\underset{\sim}{\tau}$. In practice, canceller operation deviates from these conditions, particularly because starting transients will be associated with each new set of parameter values fed to the canceller. Also, stability problems arise with a recursive filter which may make its use undesirable. An alternative possibility is to carry out multipath cancellation in the DFT domain. Analogous to the starting transient of a recursive filter, this results in a residual error which is greatest near the beginning of the reconstructed waveform. This effect can be compensated for by dropping points off the leading end of the reconstructed waveform. As an example, using N=256 samples of a modem signal with multipath at $\alpha = 0.5$, $\tau = 20$ T/N, and basing the cancellation on the exact multipath parameters, an r.m.s. signal-to-interference ratio over all 256 points of only 14 db was obtained. However, a 1 db improvement accompanied every 4 points dropped, with S/I $\underset{\sim}{>}$ 30 db when only 196 points were retained.

4.2.4 Signal Design [3],[8]

In addition to the computer programming and modem tests which have been discussed in the preceding Sections, another major area of activity has been that of signal design. Whereas the tests with the various data modems were carried out with the idea that multipath compensation would be performed strictly as supplementary to the normal operation of an existing system, the question addressed in the signal design effort was this: What is the best (or a good) transmitted waveform to be used if a complete system design is to be pursued. In the following paragraphs is outlined the general

approach which has been taken to the problem of signal design for multipath channels.

It is assumed that the received signal is disturbed by discrete multipath components which can be assumed constant over one observation period (a sequence of N samples), and that the multipath parameters needed for cancelling or reducing the multipath distortion are estimated either in part or in total by cepstrum calculations.

The signal design problem is therefore to minimize cepstrum variability due to the transmitted signal, in order that the multipath parameters become as clearly discernible in the cepstrum domain as possible. For instance, the signal cepstrum might be made zero, or close to zero, over that portion of the t'-domain which contains the detection window - the portion needed for detecting multipath and estimating the multipath parameters.

A signal with a small real cepstrum is one whose Fourier transform has approximately constant magnitude over the frequency range of interest. In order to transmit information by means of such signals, the transmitted information must therefore reside essentially in the phase spectrum of the signal. This can be accomplished by generating, within time intervals of length T, transmitted signals x(t) as a convolution,

$$x(t) = x_p(t) * x_m(t), \tag{4-2}$$

where $x_p(t)$ is a pulse shape giving rise to a suitably flat spectrum, and x_m is an all-pass modulating sequence, $x_m(t) = \Sigma\, a_i \delta(t - iT_m)$. This modulating sequence is obtained through a suitable transformation of the data sequence to be transmitted. Such a transformation is obtained if the message sequence is used directly to define a phase sequence in the frequency domain. Thus, let

$$\left.\begin{aligned} d_{x_p}(n) &\approx 1, \qquad n = 0, \ldots, N-1 \\ d_{x_m}(n) &= e^{j2\pi Q(n)}, \end{aligned}\right\} \tag{4-3}$$

where Q(n) represents a data sequence. Then, after forming $d_x(n) = d_{x_p}(n) \cdot d_{x_m}(n)$, the inverse DFT can be applied and a time waveform produced by a suitable smoothing.

The details require a careful examination of suitable ways of computing the cepstrum, and of various properties associated with different versions of cepstra. For this reason, various definitions of real and complex cepstra were established, compared, and studied in detail, as presented in [3]. This included modifications and extensions of previous developments to include practical considerations such as bandwidth and time-duration limitations. It could then be shown that the proposed signaling scheme does not require sampling synchronization between the receiver and transmitter. However, frame synchronization is required; that is, a received data sequence must be derived from only a single transmitted waveform of the type (4-2). A careful examination of this synchronization requirment, and of the effects of overlap between successive transmissions has not been made as yet.

4.2.5 Effects of Additive Noise

The effect in the cepstrum due to additive noise in the time domain was investigated in a related project [2]. This work was carried out by means of computer simulation, using APL. A brief summary is presented in Appendix F. The empirical formula (F-2) presented there was applied to the error analysis in Appendix D.

No tests with additive noise were performed with the experimental setup and PDP-8 cepstrum processor.

5. CONCLUSIONS

a) The basic objective of implementing an on-line cepstrum processor, for detecting the presence of a single multipath component in a baseband signal and estimating its magnitude and delay, was accomplished.

b) Only a very limited amount of testing was possible. However, since the test-setup and computer programs continue to be available, it would be possible to run an extended series of tests under a variety of controlled conditions, and thus obtain more comprehensive and reliable performance data.

c) On the basis of the limited test data which was obtained, a rather marginal performance was observed. A major source of error (timing jitter in sampling) was not recognized until after the project terminated. With additional time, its correction, as well as a number of other adjustments (such as data window shaping, or varying the domain of the logarithm function) would have produced some improvement in performance. However, based on the analysis of the effects of various sources of error, such modifications cannot be expected to result in a large reduction in the variability of multipath parameter estimates, below that observed in the test data of Appendix C. In other words, the modem signals themselves produce considerable variability in the cepstrum.

d) When this type of cepstrum processor is operated as part of a practical communication link, error in multipath cancellation will arise not only from the variability of the signal cepstrum, but from additive noise, from fluctuations of the multipath parameters with time, and from transients inherent in the cancellation system. This suggests that useful operation will hardly be feasible unless the signal cepstrum variability is carefully controlled, which is achievable through proper signal design.

e) The requirement of low signal cepstrum variability becomes even more urgent when the results presented in Appendix E are taken into account. A practical HF system would have to be able to compensate for at least two multipath components; and in that case, parameter estimation requires a rather fine discrimination between cepstrum peaks. Use of a combination of techniques (e.g., cepstrum analysis plus autocorrelation analysis) may be a viable strategy for achieving satisfactory performance.

APPENDIX A. DESCRIPTION OF PDP-8 PROGRAMS AND TEST SETUP

A.1 General Description of Programs

The basic functions which have been programmed and are available within the 4K(4096-word) core memory of the PDP-8 are itemized below. Fig. A1 shows the core allocation schedule by memory page. (Page numbers are base-8).

a) Storage of a 512-point sequence of data samples $\{x_1(k)\}_{k=0}^{511}$. (Memory pages 7-12; see also Section A.2.1.)

b) Application of a data window, and overlapping of the 512-point sequence into a 256-point sequence. That is, a new sequence $\{x(k)\}_{k=0}^{255}$ is generated, where $x(k) = \frac{1}{2}[w(k)x_1(k) + w(k + 256)x_1(k + 256)]$. (Memory page 13; see also Section A.2.2.)

c) Computation of the DFT of $\{x(t)\}$, giving $\{d_x(n)\}$. For this purpose, the complex FFT routine from the DECUS Program Library is used. Although the cepstrum computation as it is now carried out requires only the real FFT (discrete Fourier transform of a real sequence), the complex FFT was used in developing the program package in order to provide the option of carrying along the imaginary part. (Memory pages 2-6; the result of this computation appears in pages 7-10 (real part) and pages 17-20 (imaginary part). See also Section A.2.3.)

d) Computation of the logarithm of the magnitude of $\{d_x(n)\}$. (Memory pages 30-31; see also Section A.2.4.)

e) Computation of the inverse DFT (using again the complex FFT routine) to yield the real cepstrum $\{c_x(k)\}$. (See also Section A.2.5.)

f) Computation of the mean, maximum and minimum values at each of the first 40 cepstrum points, for 16 successively computed cepstra. (Memory pages 23-26; see also Section A.2.7.)

g) Threshold detection of a single multipath spike in the cepstrum, with a printout of estimated amplitude and position of the spike. (Memory pages 14-16 and 22; see also Section A.2.6.)

The main calling program for carrying out the cepstrum computation is stored in Page 1. This includes a routine for acquiring a sequence of signal samples via A/D conversion. There is also a provision for oscilloscope display of stored data, via D/A conversion.

Page		Contents	Page		Contents
0	0000	Pointer addresses; Constants	20	4000	Imaginary part of FFT result
1	0200	Main Calling Program; A/D, D/A Routines	21	4200	
2	0400	Complex FFT Routine	22	4400	Print routine
3	0600		23	4600	Cepstrum statistics routine
4	1000		24	5000	Storage of cepstrum statistics
5	1200		25	5200	Multiply routine
6	1400		26	5400	Calling program for cepstrum statistics; miscellaneous
7	1600	Storage of the first 256 signal samples and Real part of FFT result	27	5600	Arithmetic subroutines; Storage for detection
10	2000		30	6000	LOG routine
11	2200	Storage of additional 256 signal samples	31	6200	Logarithm look-up table
12	2400		32	6400	Magnetic tape routines
13	2600	Data window routine; Print routine	33	6600	
14	3000	Detection Routines	34	7000	EDIT Routine
15	3200		35	7200	
16	3400		36	7400	
17	3600	Imaginary part of FFT result	37	7600	Binary loader; RIM loader

Figure A1. PDP-8 Core Allocation.

Page 0 is reserved, in the usual manner, for constants and pointer addresses. Pages 34-37 contain the loaders and an Edit Routine devised by Capt. Russell Lemon of RADC. The Edit Routine facilitates the editing of programs and provides for various other manipulations. Finally, pages 32-33 contain routines for reading and writing onto a magnetic tape unit which is one of the I/O devices incorporated in the test setup at DICEF.

A.2 Detailed Description of Processing Steps.

A.2.1 Data Acquisition

Assume that a signal waveform has been connected to the A/D converter input, with peak values not exceeding the dynamic range of the converter. Under program control, A/D conversion is initiated and continued until a sequence of 512 signal samples (at a preselected sampling rate) has been stored in memory locations 1600 through 2577 (pages 7-12). Data acquisition occurs under control of the Main Calling Program.

A.2.2 Data Preparation

Before Fourier transformation, a data window is applied, and the 512-point sequence is split and overlapped into a single 256-point sequence. The data window which is used results in a raised-cosine weighting of the first and last 25 points of the data sequence, similarly to the window used in [1]. Specifically, if $\{x_1(k)\}$ denotes the 512-point sample sequence ($k = 0,1 \ldots, 511$), then $\{x_1(k)\}$gets multiplied by the sequence $\{w(k)\}$, where

$$w(k) = \begin{cases} 0.5(1 - \cos \frac{5k}{128} \pi), & k = 0, 1, \ldots, 25 \\ 1, & k = 26, \ldots, 486 \\ 0.5(1 - \cos \frac{5(512 - k)}{128} \pi) & k = 487, 488, \ldots, 511. \end{cases} \quad \text{(A-1)}$$

(The particular form for the argument of the cosine resulted from the fact that the trigonometric table of the FFT routine is used to obtain the cosine values.)

Splitting and overlapping the weighted 512-point data sequence results in a new sequence $\{x(k)\}$ $(k = 0, 1, \ldots, 255)$, where

$$x(k) = \frac{1}{2} [w(k)x_1(k) + w(k + 256)x_1(k + 256)]. \quad \text{(A-2)}$$

The factor $\frac{1}{2}$ is needed to avoid overflow. These operations are carried out by the subroutine WINDOW, which deposits the final result {x(k)} in memory locations 1600 through 2177 (pages 7 and 10).

A.2.3 Discrete Fourier Transform

The discrete Fourier transform of the sequence {x(k)} is computed using the FFT routine for complex data which is available through the DECUS Program Library [5]. The result is a complex sequence $\{d_x(n)\}$ $(n = 0, 1, \ldots, 255)$. It includes a scale factor (a power of 2) which is automatically assigned by the FFT routine in order to utilize the limited word size as effectively as possible, thus giving a quasi floating-point effect. However, this scale factor becomes merely an additive constant upon taking the logarithm, and therefore contributes only to the first cepstrum point, $c_x(0)$. Since $c_x(0)$ is of no significance in later processing and in fact will be arbitrarily reassigned later, it is not necessary to carry along the scale factor in question.

The FFT routine operates on data stored in memory pages 7, 10, 17 and 20. It considers pages 7 and 10 the real part of the input data, and pages 17 and 20 as the imaginary part. However, in the present program package only real inputs are provided for, and only the real cepstrum is computed, so that the FFT routine is used only for real data. Therefore, pages 17 and 20 are set to zero prior to execution of the FFT routine. The real part of the result of the FFT computation resides in pages 7 and 10, the imaginary part in pages 17 and 20.

A.2.4 Logarithm of Absolute Magnitude

In the LOG subroutine, first the squared magnitude of $\{d_x(n)\}$ is computed, by squaring, and then summing, the real and imaginary parts for each n. (The square root is not taken, since it amounts to merely a scalar factor after taking the logarithm, and this becomes part of the scaling performed in the cepstrum domain.) The additional 12 digits which appear in the MQ (multiplier quotient) register after squaring are carried along and used in the logarithm computation, so that no truncation error is incurred in this step.

The logarithm is computed using a look-up table for the seven most significant digits, which yields the mantissa, and the number of leading zeros

gives the characteristic. This is illustrated in Fig. A2. It is the binary logarithm which is actually computed, so that another scale factor must be applied in the cepstrum domain in order to achieve the same result as would be obtained with the natural logarithm.

The result of the logarithm computation, the sequence $\{\ell_x(n)\}$, is stored in pages 7 and 10.

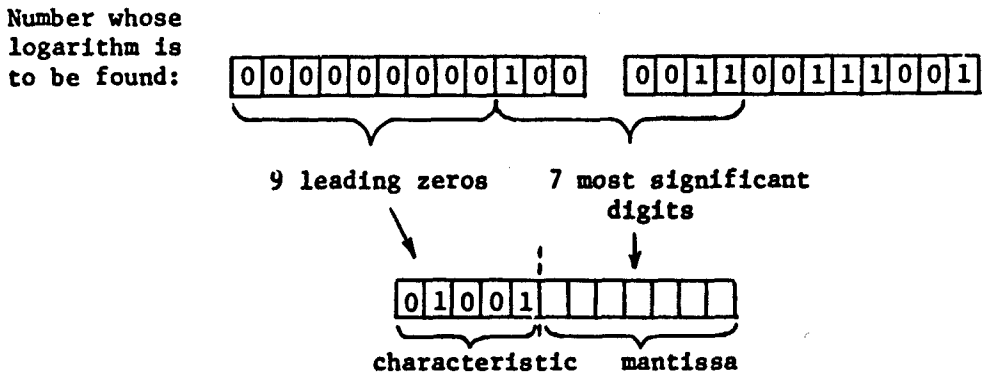

Fig. A2. Logarithm Computation

A.2.5 The Real Cepstrum

The real cepstrum is obtained by performing the inverse DFT on the real logarithm, using the FFT routine in the manner described in Section A.2.3.

In order to achieve maximum resolution in the result of the FFT computation, the output sequence should not have excessively large peaks so that advantage can be derived from the automatic scaling introduced by the FFT routine (see Sec. A.2.3). Usually, in cepstrum computation, a very large value of $c_x(0)$ is obtained, due to the d.c. component in $\{\ell_x(n)\}$. In order to avoid this large peak in the cepstrum, the log spectrum has to be shifted to make its d.c. component zero, before the inverse DFT is computed. This step is carried out in the LOG routine.

The scale factor introduced in the FFT routine during the inverse DFT computation must be corrected for in the cepstrum.

The processing steps described in Sections A.2.1 through A.2.5 are all executed under control of the Main Calling Program.

A.2.6 Detection of Multipath

The purpose of the Detection Routine is to decide whether or not multipath is present and, if the decision is that multipath is present, to estimate the multipath amplitude and delay (assuming a single discrete multipath component). The Detection Routine can be executed independently, or it can be brought under the control of the Main Calling Program.

The Detection Routine consists of the Detection Calling Program and the following subroutines:

a) Threshold Comparison Routine

b) α-Estimation Routine.

The Detection Calling Program applies all the required scale factors to the real cepstrum sequence residing in pages 7 and 10, except for the factor ln 2 = .693 which converts the binary logarithm to the natural logarithm (see Sec. A.2.4). Let the result obtained after scaling be denoted $\{c_k\}$ (k = 0, 1, ..., 255). The program then subtracts from the first $100_8 = 64$ cepstrum points the sequence of mean values $\{\bar{c}_i\}$ (i = 0, 1, ..., 63) which are stored in locations 5000 - 5077 (See Sec. A.2.7) and deposits the resulting sequence $\{c_i'\} = \{c_i\} - \{\bar{c}_i\}$ (i = 0, 1, ..., 63) in locations 1600 - 1677. The Threshold Comparison Routine is then executed.

A.2.6.1 Threshold Comparison

The sequence $\{c_i'\}$ is compared against the two threshold sequences $\{\theta_i^+\}$ and $\{\theta_i^-\}$ (see Sec. A.2.7) which are stored in locations 5100 - 5277. This results in the sequence $\{q_i\}$ (i = 0, 1, ..., 63) defined as follows:

$q_i = 0$ for each i such that $\theta_i^- \leq c_i' \leq \theta_i^+$

$q_i = c_i' - \theta_i^+$ for each i such that $c_i' > \theta_i^+$

$q_i = \theta_i^- - c_i'$ for each i such that $c_i' < \theta_i^-$.

$\{q_i\}$ is entered into locations 5600 - 5677. The largest number in the sequence $\{q_i\}$, $\max_i q_i$, is then determined, and the corresponding subscript i = i. If $\max_i q_i = 0$, then the message "NO MP" (no multipath) is typed out on the typewriter and execution terminates.

If max $q_i > 0$, execution proceeds on the assumption that a multipath spike has been detected. On the typewriter the cepstrum value $c'_{\hat{i}}$ and its storage location $(1600 + \hat{i})$ is typed out for reference. The two numbers c'_j $(j = \hat{i}+1, \hat{i}-1)$ are then examined to determine whether either one satisfies the following three requirements:

a) same polarity as $c'_{\hat{i}}$,

b) $q_j > 0$,

c) $q_j = \max_{\ell} q_\ell$, $(\ell = \hat{i}+1, \hat{i}-1)$.

If this test is satisfied by either j-value, denote it $\hat{j}$. The numbers $\hat{j}$ and $c'_{\hat{j}}$ are stored. The program then jumps to the α-Estimation Routine.

A.2.6.2 α-Estimation Routine

If no $\hat{j}$ is stored, α is estimated from $c'_{\hat{i}}$ only. That is, estimation of α proceeds on the assumption that τ is exactly equal to $\hat{i}$ sampling intervals. The estimate of α is then

$$\underset{\sim}{\alpha} = \frac{.693\ c'_{\hat{i}}}{N/2}, \tag{A-3}$$

and the estimate of τ is $\underset{\sim}{\tau} = \hat{i}/f_s$, where $f_s = T/N$ is the sampling frequency.

On the other hand, if $\hat{j}$ has been stored, then the α-estimate is based on both $c'_{\hat{i}}$ and $c'_{\hat{j}}$, and an interpolation between $c'_{\hat{i}}$ and $c'_{\hat{j}}$ is performed as described in Sec. 2.4. That is, let

$$\phi = |c'_{\hat{j}}| \ / \ (|c'_{\hat{i}}| + |c'_{\hat{j}}|).$$

Then the α-estimate is

$$\underset{\sim}{\alpha} = \frac{c'_{\hat{i}} \times 2 \times .693}{N \operatorname{sinc} \phi} \tag{A-4}$$

and the estimate of τ is

$$\underset{\sim}{\tau} = \frac{\hat{i} + (\hat{j} - \hat{i})\phi}{f_s}\ . \tag{A-5}$$

(The present version of the program does not provide for explicit computation of τ.)

A typewriter printout is then generated, which lists α, $\hat{i}$, $\hat{j}$ (if it exists), $|c'_{\hat{i}}|$, $|c'_{\hat{j}}|$, and $|c'_{\hat{i}}|/\text{sinc}\,\phi$. Thereafter the Detection Routine terminates.

A.2.7 Cepstrum Statistics

The Detection Routine requires mean cepstra and thresholds for any given type of modem signal. Using a separate Calling Program, statistics can be compiled for the first $100_8 = 64$ cepstrum points for a set of 16 signal sequences. This Calling Program cycles through the Main Calling Program 16 times in succession, and processes the first 64 points of each of the 16 cepstra thus obtained to yield

a) a mean cepstrum (estimate) for the given signal source, $\{\bar{c}_i\}$, $i = 0, 1, \ldots, 63$
b) the sequence of maximum values
c) the sequence of minimum values (negative maxima)

The sequence $\{\bar{c}_i\}$ is entered into locations 5000 - 5077, the maxima in locations 5100 - 5177, the minima in locations 5200 - 5277. The mean values are used directly by the Detection Routine (Sec. A.2.6). The minima and maxima can be used to establish thresholds. However, this has not been programmed; instead, thresholds have been entered manually for the various test runs.

A.3 The General Test Setup

In order to perform on-line cepstrum analysis of communication signals, the PDP-8I at DICEF was operated in connection with other equipment as illustrated in Fig. A3. A data modem is driven from a transmission test set which generates a long pseudo-random binary modulating sequence. The baseband output of the modem is returned to the baseband input for demodulation and the resulting data stream returned to the transmission test set, for an error check. This connection allows verification that a proper baseband output is derived from the modem.

The modem output is also fed through the DICEF Wireline Simulator which is programmed to introduce the desired multipath interference. (For cepstrum computations of the undistorted modem signal, the wireline simulator is bypassed). Since the conversion range of the A/D converter is $\pm$ 10 V, the

Wireline Simulator output is passed through variable attenuation and an amplifier.

A/D conversion takes place under program control. That is, conversion of a sequence of samples is initiated when the computer is ready to accept the data. A square wave generator connected to the A/D converter determines the sampling rate.

Oscilloscope observation of stored data, such as a cepstrum sequence, is possible through a D/A routine which reads out the desired data sequence respectively to a D/A converter. The oscilloscope is connected to the D/A converter output.

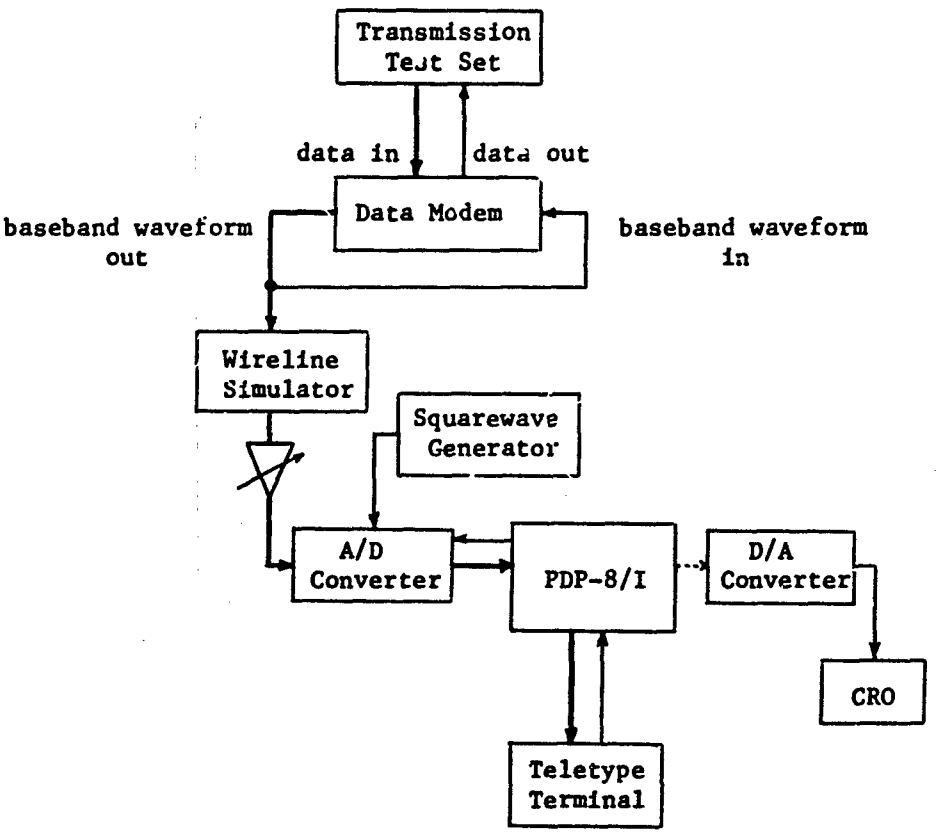

Fig. A3 Test Setup

APPENDIX B. SOURCES OF ERROR

B.1 Accumulated effect of truncation error in the cepstrum

The accumulated effect of truncation errors which occur in the FFT and logarithm computations was examined by computing the cepstrum of a signal sequence both via PDP-8 and also via APL\370. For this purpose, a 512 point sample sequence derived from a USC-9 modem, with multipath, was first subjected to the WINDOW routine (that is, the data window was applied and the sequence was folded over into 256 points.) The resulting 256-point sequence, in 4-digit octal representation, was typed into the APL terminal, converted to decimal form, and its cepstrum computed. The cepstrum was also computed via PDP-8. The APL computation yields the cepstrum with negligible error due to truncation. Comparison of the two cepstra thus obtained was accomplished by again copying the PDP-8 result into APL, and computing the difference of the two cepstra. The resulting error sequence (excluding the initial point) was characterized by the following parameter values:

Peak error: 0.755
RMS error: 0.267

These values must be divided by N/2 = 128 in order to relate them to $\underset{\sim}{g}$, the estimated multipath amplitude. Thus, if the peak error of 0.755 were to occur at exactly that point in the cepstrum where the largest multipath spike is located, and assuming that the multipath delay τ is an exact multiple of the sample spacing, then this peak truncation error will contribute an error of $\pm 0.755/128 \approx \pm 0.006$ to $\underset{\sim}{g}$. The r.m.s. error in $\underset{\sim}{g}$ due to truncation, on the basis of this single test, is, therefore, $0.267/128 \approx 0.002$, which is small.

This result must be accepted with some reservations, however. The amplitude distribution of $\{d_y(n)\}$, the DFT sequence, can vary noticeably for different input sequences from the same source. This distribution affects the magnitude of the truncation error, that is, more truncation error is associated with the very small values of $\{d_y(n)\}$.

B.2 Error introduced in Data Preparation

The truncation error check described in the preceding section does not account for error introduced during data preparation using the WINDOW routine (see Sec. A.2.2). Truncation errors are introduced in the representation of

cosine values, the multiplication, and the scaling. However, the errors due to the truncated representation of the cosine values are not variable, since a fixed look-up table is used. Therefore, they do not contribute to the variability of the α-estimate. The same statement applies to the w(k)'s in (A-1).

Scaling and overlapping, as indicated in (A-2), results in an error distribution at each sample point as shown in Fig. B1, which has a variance of 1/8. At each of the first and last 25 points of the resulting 256-point sequence, one of the two numbers being added is the result of a multiplication and, therefore, has sustained an additional truncation error. The error distribution at these points is therefore approximately of the form shown in Fig. B2, and has a variance of 7/48. But this value only applies at approximately 20% of the 256 points and does not differ greatly from 1/8, so that the total error introduced in conditioning the input sequence has a variance of approximately 1/8. The corresponding error standard deviation is $\sqrt{1/8} = 0.35$.

This error represents additive noise at the input to the cepstrum processor. Its effect on the cepstrum can be estimated by the method of Appendix F.

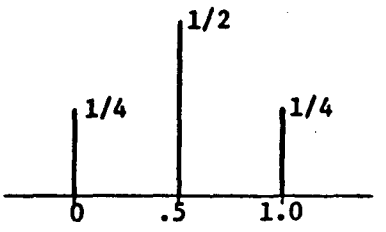

Figure B1
Error Distribution

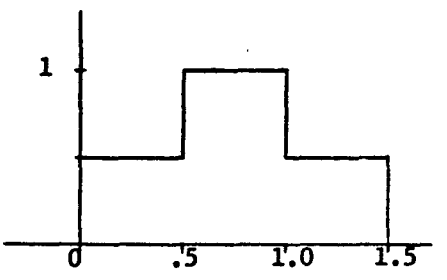

Figure B2
Error Distribution

B.3 Effect of Signal Quantization

The effect of signal quantization on the cepstrum was explored by computing the cepstrum of the same signal sequence several times, but each time dropping an additional digit in the binary representation of each input signal sample. Thus, a 256-point signal sequence was recorded on paper tape, and its

cepstrum computed. The same signal sequence was then again read into the PDP-8, a right-shift of one digit applied, and the cepstrum computed. (The FFT-routine automatically adjusts its input for maximum dynamic range, so that the effect of the right shift is essentially to convert the least significant digit to zero.) This was repeated with a right shift of 2 digits, 3 digits, etc.

The test was applied to three different signal sequences derived from the USC-9 modem with multipath of $\alpha = 1/2$, $\tau = 1.6$ ms, at a nominal sampling rate of 7000 Hz. Comparison of the cepstra was restricted to the region $1 \leq k \leq 40$ which is approximately the region of interest for multipath detection. Over this region, the rms error of the cepstrum with truncated input (compared to the cepstrum without input truncation) was determined for each of the conditions tried. The results are shown in Figs. B3-B6. Figures B3-B5 display the discrepancies between the cepstrum based on the quantized representation and the cepstrum computed from the 12-bit representation of the signal. For each of the three signals and for any given number of binary digits dropped, a histogram is presented showing the number of cepstrum points which differed by 0, by 1, by 2, etc. The units in these figures are based on the binary logarithm; that is, they are the units in which the Main Calling Program generates the cepstrum (Sec.A.2.5). The scales in these Figures have to be multiplied by $\ln 2 = .693$ in order to bring them in agreement with the usual amplitude scale used for cepstra.

This scale factor was incorporated in Figure B6, where the r.m.s. cepstrum error for each of the three signal samples is plotted as a function of the number of digits dropped at the input. While for the signal sequences "A" and "B" there is relatively little effect produced by dropping up to 4 digits, signal "C" shows significant spectrum degradation even upon dropping a single digit. One can assume that with the 12-bit A/D conversion actually used, the quantization error produced little effect in the cepstra of signals "A" and "B", but a noticeable effect in the case of signal "C". Clearly, some signal sequences are much more "error-prone" than others.

It is possible that signal C (after overlapping) had a sufficiently larger peak value than the others, so that the FFT routine applied a different scale factor, thus essentially introducing additional truncation error. But

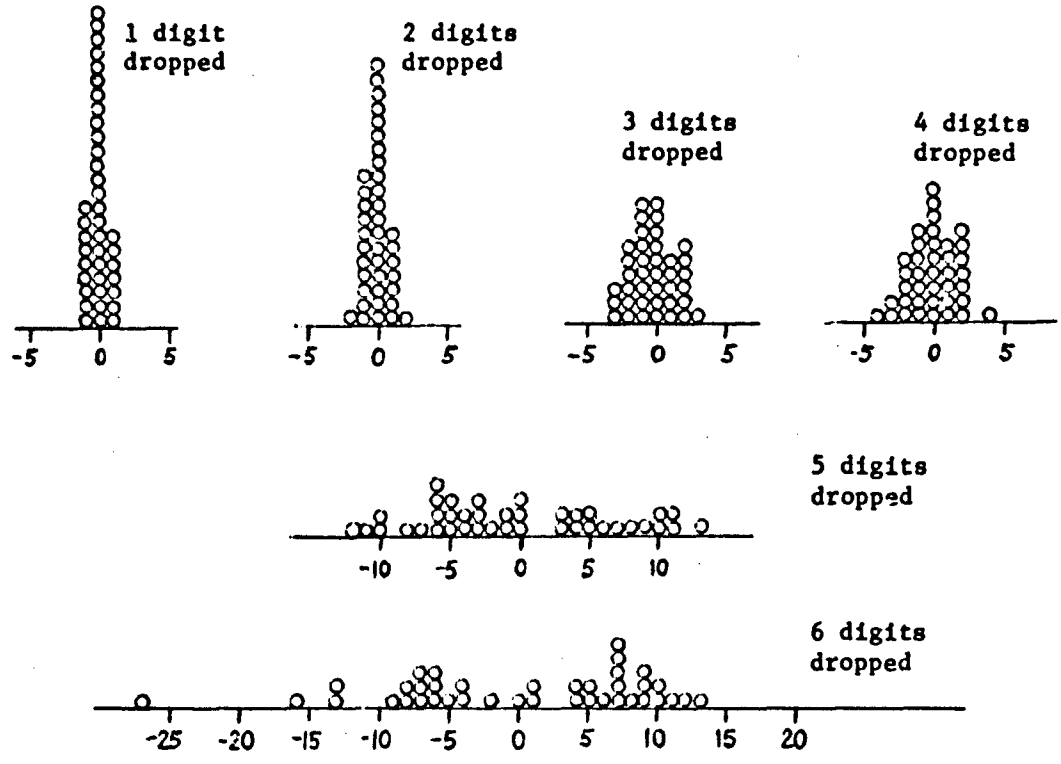

Figure B3. Cepstrum errors resulting from successively coarser quantization. Signal sample A.

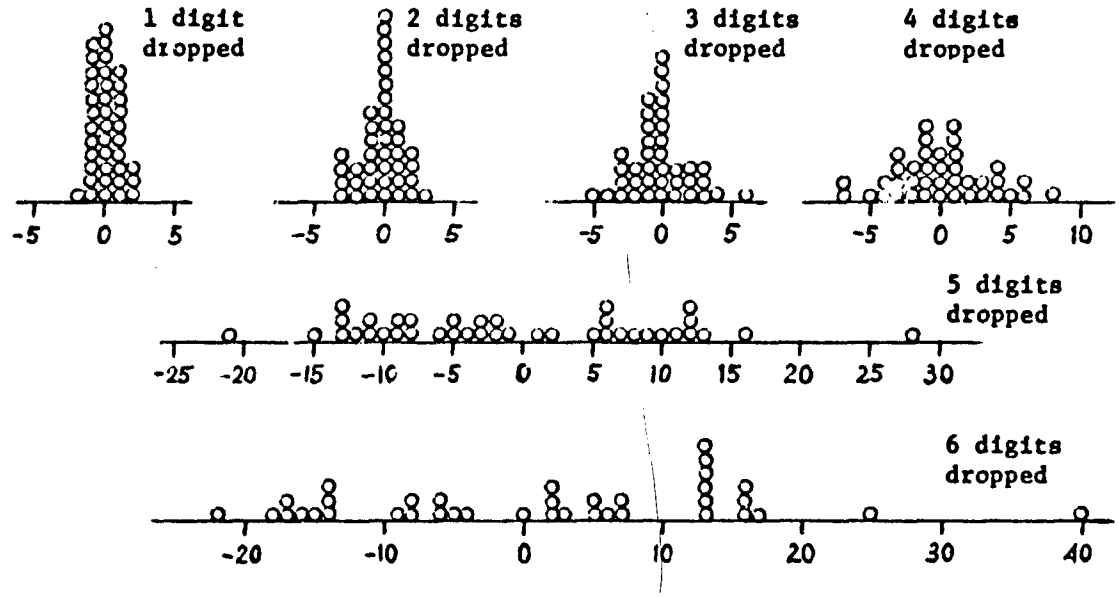

Figure B4. Cepstrum errors resulting from successively coarser quantization. Signal sample B.

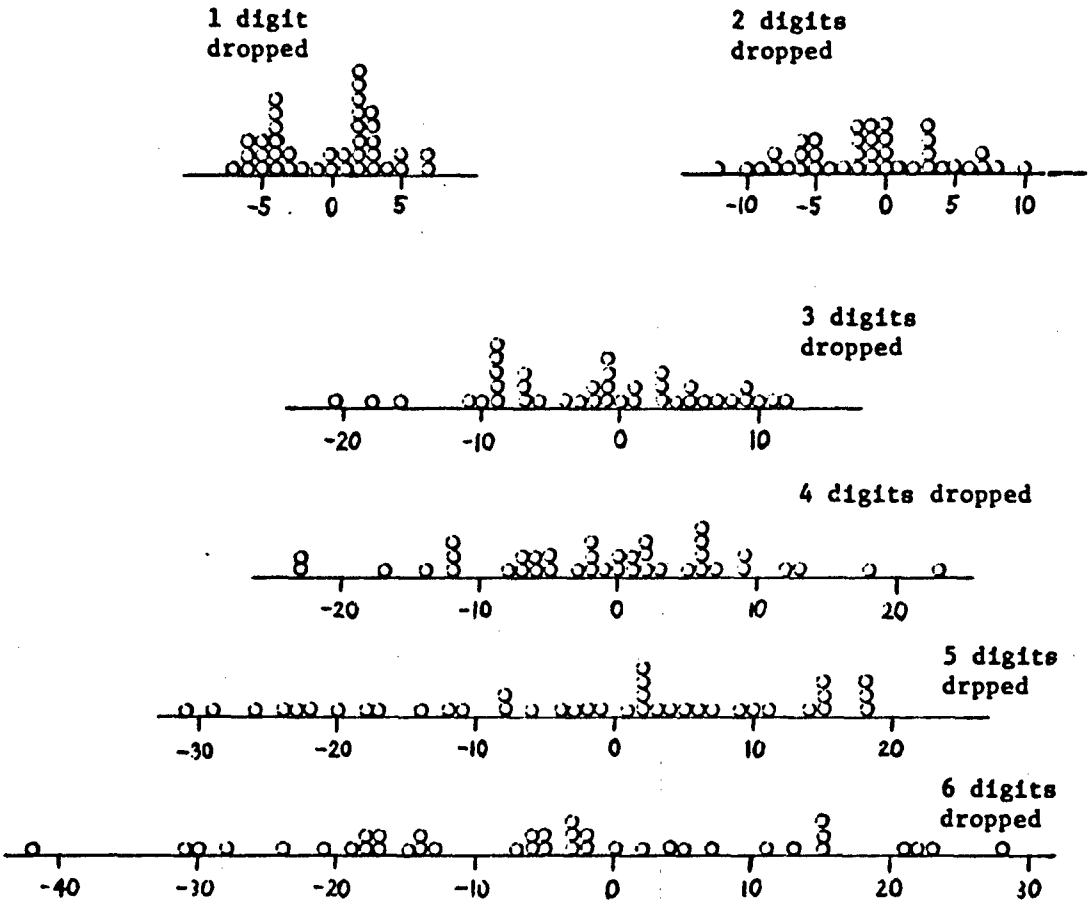

Figure B5. Cepstrum errors resulting from successively coarser quantization. Signal Sample C.

it is more likely that the different results obtained with this signal are due to the same effect mentioned at the end of Section B.1. Thus, the DFT of the signal C may have more points close to zero, thus aggravating the effect of slight changes in input signal.

In Figure B.6 are also shown, for comparison, estimates of r.m.s. cepstrum error as obtained from equation (F-2).

The errors which are plotted in Figures B3-B5 were in each case quite randomly distributed over the region of the cepstrum which was examined. The cepstrum locations containing the multipath spike were not affected in

a unique way. The α-estimates derived from the various runs are as follows:

digits deleted	Signal		
	A	B	C
none	.445	.445	.641
1	.445	.469	.656
2	.430	.469	.641
3	.445	.484	.672
4	.430	.445	.539
5	.414	.539	.516
6	.367	.445	.484

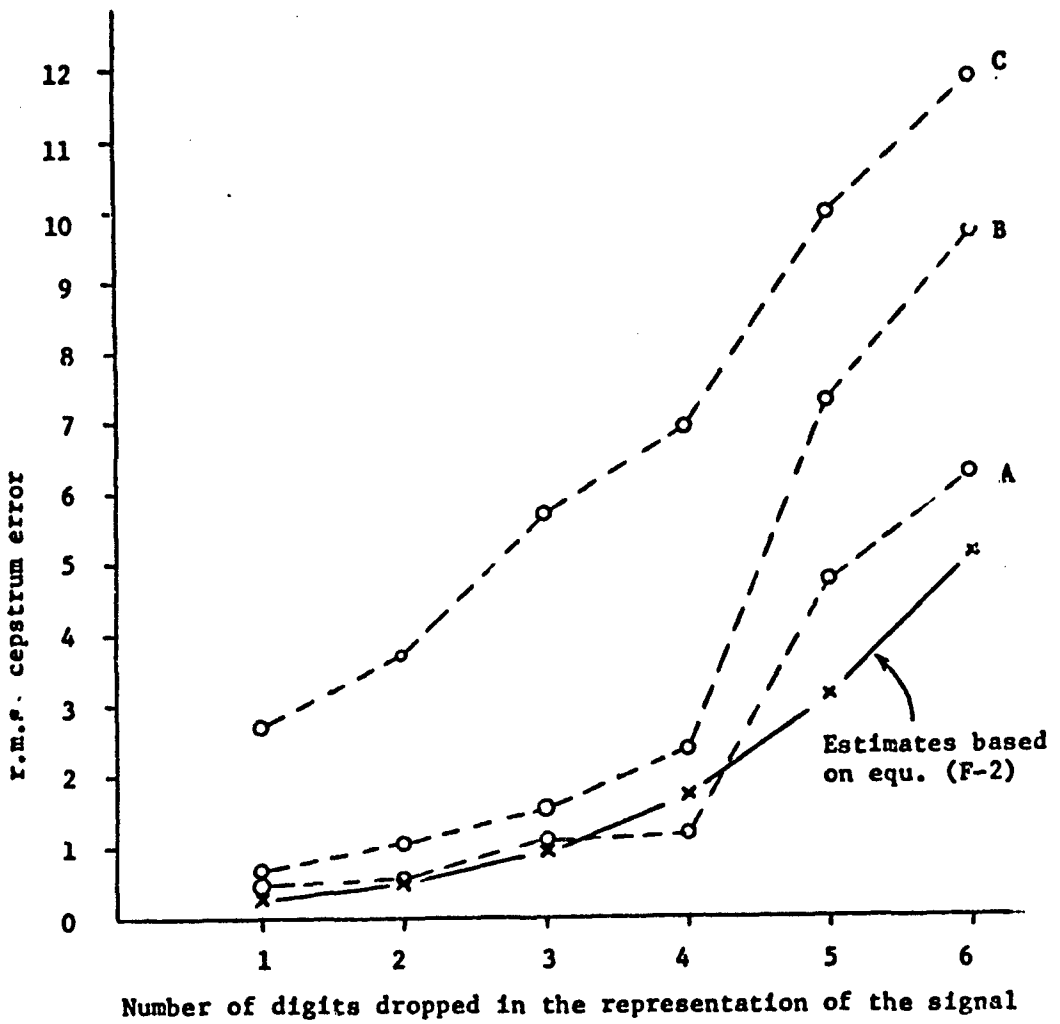

Figure B6. R.m.s. cepstrum error due to signal quantization.

B.4 Sampling Jitter

The discussion of sources of error contained in the preceding sections is useful in understanding the overall system operation and can serve to guide further program design. However, in the experimental setup, the error due to the sources which have been discussed so far was overshadowed by the error due to sampling jitter, - a fact which was recognized too late to be corrected.

The excessive sampling jitter was a result of the manner in which synchronization for the sample-and-hold module was derived. Whereas the sampling rate was set by means of a squarewave generator, the "hold" was initiated when a loop in the A/D subroutine first encountered a "positive" condition at the squarewave generator output. Therefore, the initiation of "hold" had a variable delay with respect to the positive-going edge of the square wave. The maximum value of this variation in delay is the cycle time of the software loop in question, which is the following:

Loc:	Contents	Operation:	Exec. Time
0307	6141	If input timing = 1, skip next instruction.	2.6 μsec.
0310	5307	Jump to 0307	3 μsec

Initiation of "hold" is effected by the next instruction. The maximum variation in "hold" timing is therefore 5.6 μsec.

The r.m.s. error due to sampling jitter can be determined in the following way. Let the sampling jitter be characterized by a uniformly distributed random variable, J, and let Δ denote the peak-to-peak value of the jitter. If $x(t)$ is the signal being sampled, then the sampling error at time t_o is $Jx'(t_o)$. (This expression assumes that $x'(t)$ does not vary substantially over a Δ-interval, which is true in the case being considered.) The r.m.s. jitter at t_o is therefore $(\Delta/\sqrt{12})x'(t_o)$. The r.m.s. value of the derivative of the input signal can be determined approximately from the signal sample sequence by using (B-9). The approximation is based on the simplifying assumptions of Sec. B.5. The approximate m.s. error due to sampling jitter, at the sampler output, is therefore

$$\frac{\Delta^2}{12}\left[2\sum_{n=1}^{\frac{N}{2}-1}\left(\frac{2\pi n f_s}{N}\right)^2 |d_x(n)|^2 + (\pi f_s)^2 |d_x(\tfrac{N}{2})|^2\right]. \qquad \text{(B-1)}$$

B.5 Computing the m.s. value of the derivative of a signal from the sampled signal

Consider a real signal x(t) which is sampled to give the sample sequence $\{x_k\} = \{x(\frac{kT}{N})\}$ $(k = 0, 1, \ldots, N-1)$. Its DFT is

$$\{d_x(n)\} = \{\frac{1}{N}\sum_{k=0}^{N-1} x_k e^{-j\frac{2\pi nk}{N}}\}. \qquad \text{(B-2)}$$

The "energy" of the sequence $\{d_x(n)\}$ is the m.s. value of the signal sequence

$$\sum_{n=0}^{N-1} |d_x(n)|^2 = \frac{1}{N^2}\sum_{n=0}^{N-1}\left(\sum_{k=0}^{N-1} x_k e^{-j\frac{2\pi nk}{N}}\right)\left(\sum_{\ell=0}^{N-1} x_\ell e^{+j\frac{2\pi n\ell}{N}}\right) = \frac{1}{N}\sum_{k=0}^{N-1} x_k^2. \qquad \text{(B-3)}$$

Equivalently,

$$\text{m.s. value of DFT} = \frac{1}{N} \times \text{m.s. value of signal sequence.} \qquad \text{(B-4)}$$

The inverse of the relationship (B-2) is

$$\{x_k\} = \{\sum_{n=0}^{N-1} d_x(n)\, e^{j\frac{2\pi nk}{N}}\},$$

which can also be written

$$\{x_k\} = d_x(0) + \sum_{n=1}^{\frac{N}{2}-1}\left[d_x(n)e^{j\frac{2\pi nk}{N}} + d_x(N-n)e^{-j\frac{2\pi nk}{N}}\right] + d_x(\tfrac{N}{2})e^{j\pi k}, \qquad \text{(B-5)}$$

If the signal x(t) is assumed periodic with period T, and strictly band-limited to frequencies not exceeding $\frac{N}{2T}$, then x(t) can be expressed exactly by replacing kT/N in (B-5) by t:

$$x(t) = d_x(0) + \sum_{n=1}^{\frac{N}{2}-1} \left[d_x(n) e^{j \frac{2\pi nt}{T}} + d_x(N-n) e^{-j \frac{2\pi nt}{T}} \right] + d_x(\tfrac{N}{2}) e^{j \frac{\pi Nt}{T}} \qquad \text{(B-6)}$$

The derivative of x(t) is therefore given by

$$x'(t) = \sum_{n=1}^{\frac{N}{2}-1} j\tfrac{2\pi n}{T} \left[d_x(n) e^{j \frac{2\pi nt}{T}} - d_x(N-n) e^{-j \frac{2\pi nt}{T}} \right] + d_x(\tfrac{N}{2}) j\tfrac{\pi N}{T} e^{jn \frac{Nt}{T}}. \qquad \text{(B-7)}$$

The sample sequence of the derivative, $\{x'_k\}$, then has DFT $\{d_{x'}(n)\}$ given by

$$\{d_{x'}(n)\} = \{ j \tfrac{2\pi n}{T} d_x(n) \} \qquad (n = 1 - \tfrac{N}{2}, \ \ldots \ , \tfrac{N}{2}). \qquad \text{(B-8)}$$

Using (B-3) and the symmetry in the DFT of a real sequence, the m.s. value of the derivative is found to be

$$\sum_{n=0}^{N-1} |d_{x'}(n)|^2 = \left(2 \sum_{n=1}^{\frac{N}{2}-1} (\tfrac{2\pi n}{T})^2 |d_x(n)|^2 \right) + (\tfrac{\pi N}{T})^2 |d_x(\tfrac{N}{2})|^2. \qquad \text{(B-9)}$$

B.6 Estimate of the Mean Signal Cepstrum

Estimation of multipath amplitude requires subtraction of the mean signal cepstrum from the actually observed cepstrum. Since the mean signal cepstrum is only available in the form of an estimate, it introduces an error in the multipath estimate. This is a systematic error, for a given type of signal and sampling rate (i.e., for a set of multipath estimates all of which are based on the same mean cepstrum estimate.)

A representative computation of the magnitude of this error was performed using 6 different mean-cepstrum estimates which were obtained with the USC-9 modem at 7000 samples/sec. (see Fig. C1). By averaging over cepstrum points number 3 to number 22 (corresponding to a range of τ from .43 ms to 3.14 ms) the average standard deviation of the mean-cepstrum estimates was found to be 1.93.

Another error arises due to the fact that the true mean cepstrum is actually modified somewhat if multipath is present (aside from the superposition of the multipath spikes). This error increases with both α and τ,

and is due to the end effect illustrated in Fig. 3. In order to estimate the size of this error, it is necessary to compare mean cepstra that have been obtained with multipath present (for various values of α and τ), and the mean cepstrum without multipath. This procedure also would yield measurements of the attenuation experienced by the multipath cepstrum, as discussed in Sec. 2.4. No systematic sequence of such tests was performed, however.

B.7 Detection Thresholds

The setting of the detection thresholds hinges on the probabilities of several different events:

p_m, the probability of missing the multipath spike (given that multipath is actually present)

p_{fa}, the probability of a false alarm (detecting a multipath spike given that no multipath is present)

p_w, the probability of wrong detection (detecting a multipath spike at a wrong position in the cepstrum, given that multipath is actually present)

Suppose a single multipath component is present with delay $\tau = rt_o$ and relative amplitude α. If the distribution of the signal cepstrum at point r is symmetrical and the mean has been subtracted, then $P_m = 1/2$ if $N\alpha/2 = \theta_r$. (This neglects the possibility of exceeding the reverse polarity threshold). Thus, as far as the probability of a "miss" is concerned, the setting of the threshold is guided by how small a multipath amplitude is to be detected. The larger the true α when a "miss" occurs, the more serious the error at the output of a multipath correction network which has been adjusted in accordance with the detection result.

Taking into account the possibility of false alarms is not quite so straightforward. If the thresholds are set high, then P_{fa} is small, but the false alarms which do occur will result in significant distortion when multipath cancellation is applied. On the other hand, many of the false alarms which occur under a low threshold setting will produce small α-estimates, so that less serious distortion is introduced by a multipath correction network which has been adjusted in accordance with the detection result.

A wrong detection, or detection error, occurs when some point in the cepstrum exhibits such a large excursion (due to the random nature of the signal) that it is interpreted as the multipath spike, while a multipath spike is actually present at a different point in the cepstrum, but with smaller magnitude. A wrong detection results in a double degradation in place of multipath cancellation - due to the uncorrected actual multipath and due to the compensation of a multipath component actually not present. Here again, increasing the threshold setting lowers P_w. Also, it allows only the more disruptive of such errors to occur, which are those associated with large values of $\underline{\alpha}$.

An approximate expression for P_w is obtained below by neglecting the possibility of one or more of the minor spikes of the multipath cepstrum falling within the detection window. However, the possibility is included that the cepstrum value at the location of the major multipath spike does not reach threshold.

Suppose that multipath is present with a delay equal to an integer number of sample spacings, $\tau = r(T/N)$, so that the main multipath spike is located at cepstrum point r. Let the multipath amplitude be α, so that the multipath spike has amplitude $c_m(r) = N\alpha/2 - \delta_r$. (The parameter δ_r expresses the depression of the multipath spike at point r due to the fact that multipath introduces a linear shift, not a cyclic shift.) The signal cepstrum at point r is $c_x(r)$. Thus, a detection error arises if $c_y(r) = c_m(r) + c_x(r) < c_x(k)$ for some k within the detection window such that $c_x(k) > \theta_k$.

The following simplifying assumptions will now be made:

(a) $c_x(k)$, for different k within the detection window, are independent, identically distributed random variables; a representative one of these will be denoted C.

(b) The thresholds for each k are all set to the same values, $\pm\theta$, with respect to the true mean of the signal cepstrum at point k.

Let D be the number of cepstrum points lying within the detection window. The conditional probability of error, given $c_y(r)$, (where $c_y(r) > \theta_r$) is then

$$P(E|c_y(r)) = 1 - \{F_C[c_y(r)] - F_C[-c_y(r)]\}^{D-1}. \quad \text{(B-10)}$$

The probability of a detection error, given $c_m(r)$, is then

$$P_w = \int_{\theta_r - c_m(r)}^{\infty} P(E|c + c_m(r)) f_C(c)dc + p_o\{1 - [F_C(\theta) - F_C(-\theta)]^{D-1}\}. \quad \text{(B-11)}$$

In this expression, p_o is the probability of the event $c_y(r) \leq \theta_r$. A slightly simpler expression than (B-11) is obtained for the combined probability of a miss or a detection error:

$$P_m + P_w = \int_{\theta_r - c_m(r)}^{\infty} P(E|c + c_m(r)) f_C(c)dc + p_o. \quad \text{(B-12)}$$

If (B-12) is computed for the case where the C's are gaussian random variables with standard deviation σ, and with $\delta_r = 0$, the following representative values are obtained:

	$\theta = 2\sigma$	$\theta = 2.5\sigma$
$\alpha = 3\sigma$, $D = 31$	.128	.047
$\alpha = 3\sigma$, $D = 16$	.074	.025
$\alpha = 4\sigma$, $D = 31$	.046	.024
$\alpha = 4\sigma$, $D = 16$	.026	.0124
$\alpha = 5\sigma$, $D = 31$	.0072	.0050
$\alpha = 5\sigma$, $D = 16$	.0039	.0026

This set of computed values illustrates the following points:

a) There is a significant penalty associated with allowing too large a detection window. The detection window should not be wider than required to accommodate the expected range of τ.

b) The value of σ is of great importance. For instance, going from $\{\theta = 2\sigma, \alpha = 4\sigma\}$ to $\{\theta = 2.5\sigma, \alpha = 5\sigma\}$ corresponds to reducing the

variability of the signal cepstrum by 33%, and results in a reduction in $P_m + P_w$ by a factor of 10, approximately.

The false alarm probability, P_{fa}, is given by the following approximate expression, based on the above assumptions:

$$P_{fa} = 1 - \left[\int_{-\theta_r}^{\theta_r} f_C(c)dc \right]^D \qquad \text{(B-13)}$$

APPENDIX C. RESULTS OF TEST RUNS

Cepstrum statistics were collected, and multipath detection runs performed, using signals from three different types of modems: a USC-9 modem, a Codex 9600 modem, and a Hughes HC-276 modem. The test setup for all tests was as described in Section A3. Analysis of the test data is contained in Appendix D.

C.1 The USC-9 Modem

The USC-9 was operated at a data rate (serial binary input) of 2400 bits/sec. Its output consists of four quadraphase PSK channels centered at different frequencies within the audio band.

C.1.1 Cepstrum Statistics

Cepstrum statistics were collected at several different sampling frequencies ($f_s \cong$ 5800, 6000, and 7000 Hz). The mean cepstra obtained in this manner were used in order to perform multipath detection runs at each of these sampling frequencies. With $f_s \cong$ 7000 Hz, six independent computations of cepstrum statistics were made, in order to examine the variability of the estimates which are obtained. Fig. C1 shows the ranges of cepstrum maxima, minima, and mean values for the six different computations. The solid line connects that particular set of cepstrum mean values which was used in the multipath detection runs at $f_s \cong$ 7000 Hz.

C.1.2 Multipath Detection

Test runs were made at sampling frequencies of $f_s \cong$ 5800, 6000, and 7000 Hz. Multipath detection runs at each of these values of f_s utilized the mean cepstrum computed for that sampling frequency. The same threshold settings were used for all detection runs, with rather low threshold values and with the detection window extending over cepstrum samples No. 1 through 39. The multipath parameters in all these runs were $\alpha = 0.5$, $\tau \cong 1.6$ ms. The α-estimates which were obtained are plotted in Fig. C2. No correction for the multipath spike depression discussed in Sec. 2.4 was applied to this data. Those runs which resulted in detection based on an incidental cepstrum peak (at an incorrect value of τ) are indicated in the column marked "detection error".

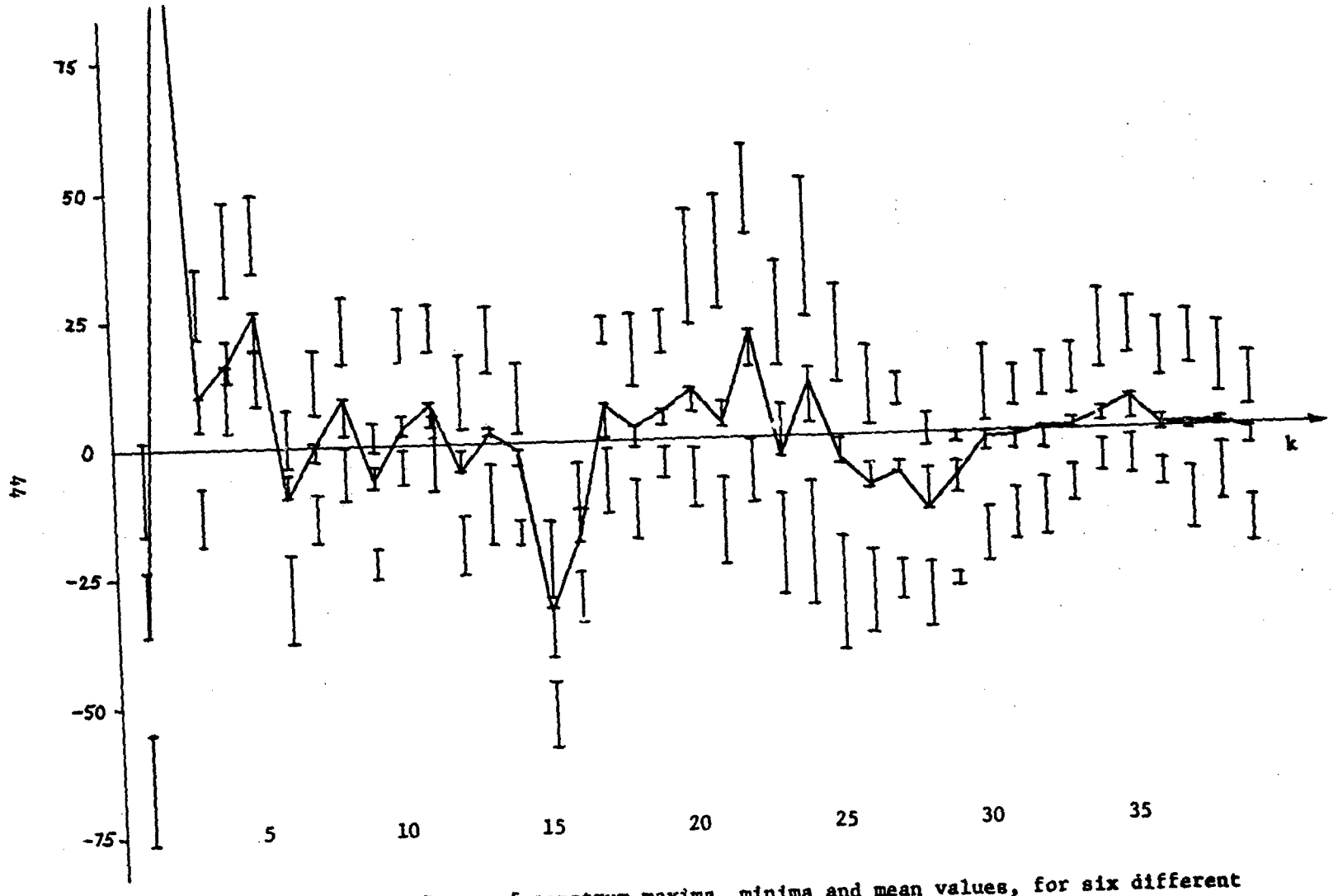

Figure C1. USC-9 Modem: Range of cepstrum maxima, minima and mean values, for six different sets of 16 cepstra, with f_s = 7000 Hz.

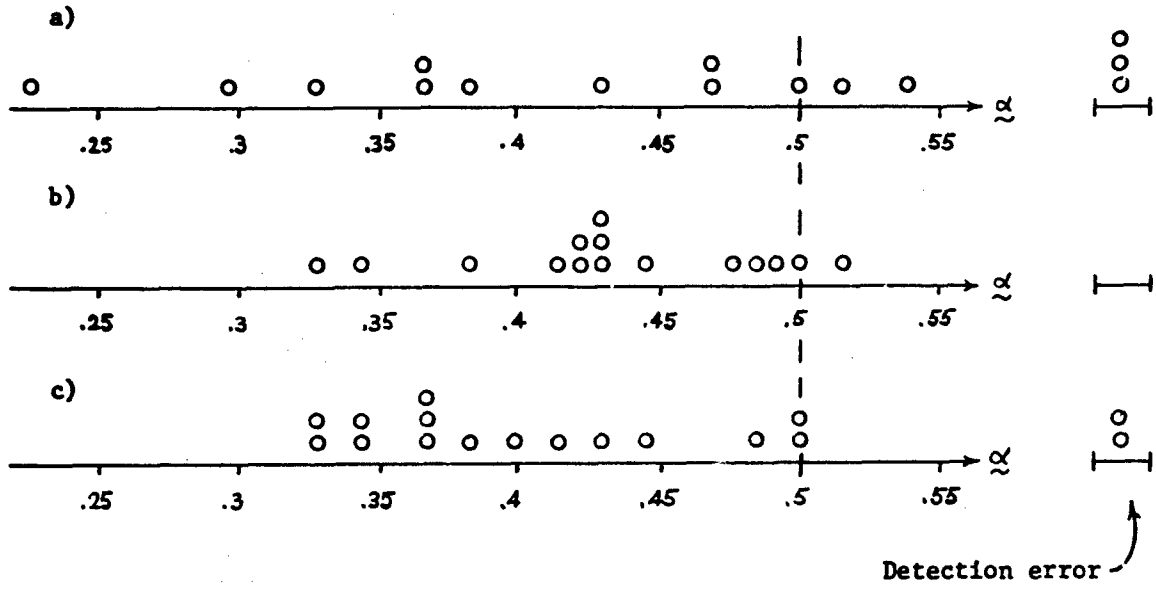

a) f_s = 5800 Hz; b) f_s = 6000 Hz; c) f_s = 7000 Hz.

Figure C2. Multipath Detection at different Sampling Rates - USC-9 Modem. Estimates of α, (true α = 0.5).

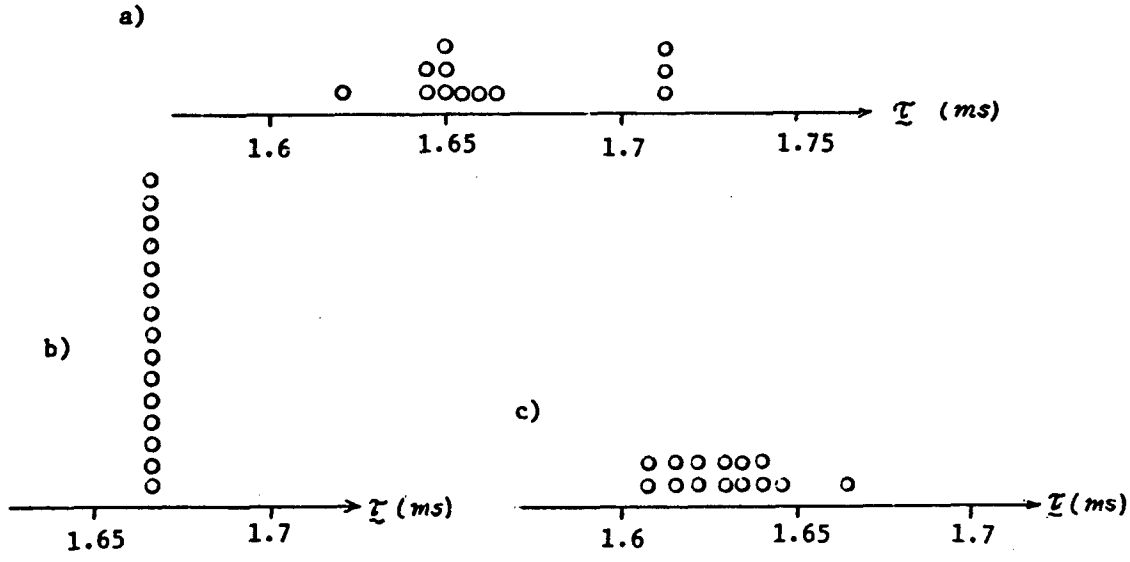

a) f_s = 5800 Hz; b) f_s = 6000 Hz; c) f_s = 7000 Hz

Figure C3. Multipath Detection at different sampling rates - USC-9 Modem. Estimates of τ, with α = 0.5.

Estimates of τ obtained by applying (A-5) to the data, are plotted in Fig. C2. These computations were done in APL, since the PDP-8 programs do not give $\underset{\sim}{\tau}$. The results shown in Fig. C3 can only be interpreted on a relative basis for each sampling rate because in the tests, a precise adjustment (or measurement) of the sampling rate with respect to the true multipath delay was not attempted. Thus, with 6000 samples per second (Fig. C3-b) the multipath delay was sufficiently close to an exact multiple of the sample spacing that in none of the cases was the threshold reached at a point adjacent to the maximum cepstrum peak. The same value of $\underset{\sim}{\tau}$ was therefore obtained in all cases, namely $\underset{\sim}{\tau} = \hat{i}/f_s$ where $\hat{i}$ is the position of the largest cepstrum peak. (See also Sec. D.1 for further discussion of the effect of the threshold setting on $\underset{\sim}{\tau}$.)

C.2 The Codex 9600 Modem

This modem uses combined phase and amplitude modulation of a single subcarrier. The modem handles a maximum data rate of 9600 bits per second, but it was operated at 4800 bps in the tests which were performed. The variability of the signal cepstrum was found to be similar as for the USC-9 and HC-276 modems.

C.2.1 Detection Runs

An extensive set of detection runs was carried out under the following conditions: $\alpha = 0.5$, $\tau = 2.9$ ms., $f_s \cong 7000$ Hz. With this combination of τ and f_s, the multipath delay does not correspond to an integer number of sample spacings. The results are plotted in Figs. C4, C5 and C6. A total of 201 multipath estimates were computed, of which 25 resulted in a detection error. There were no misses. Fig. C4 shows the distribution of α-estimates (including detection errors) without correction for multipath cepstrum depression. Fig. C5 shows the distribution of τ-estimates, again excluding detection errors. The horizontal scale in this Figure assumes a sampling frequency of exactly 7000 Hz. Under this assumption, cepstrum sample # 20 corresponds to $\tau = 2.857$ ms, and cepstrum sample #21 corresponds to $\tau = 3.00$ ms. Since the existing Detection Routine does not compute τ-estimates, the data for Fig. C5 was computed on APL, and the horizontal scale of the plot was quantized to increments of .05. The estimates in the range from

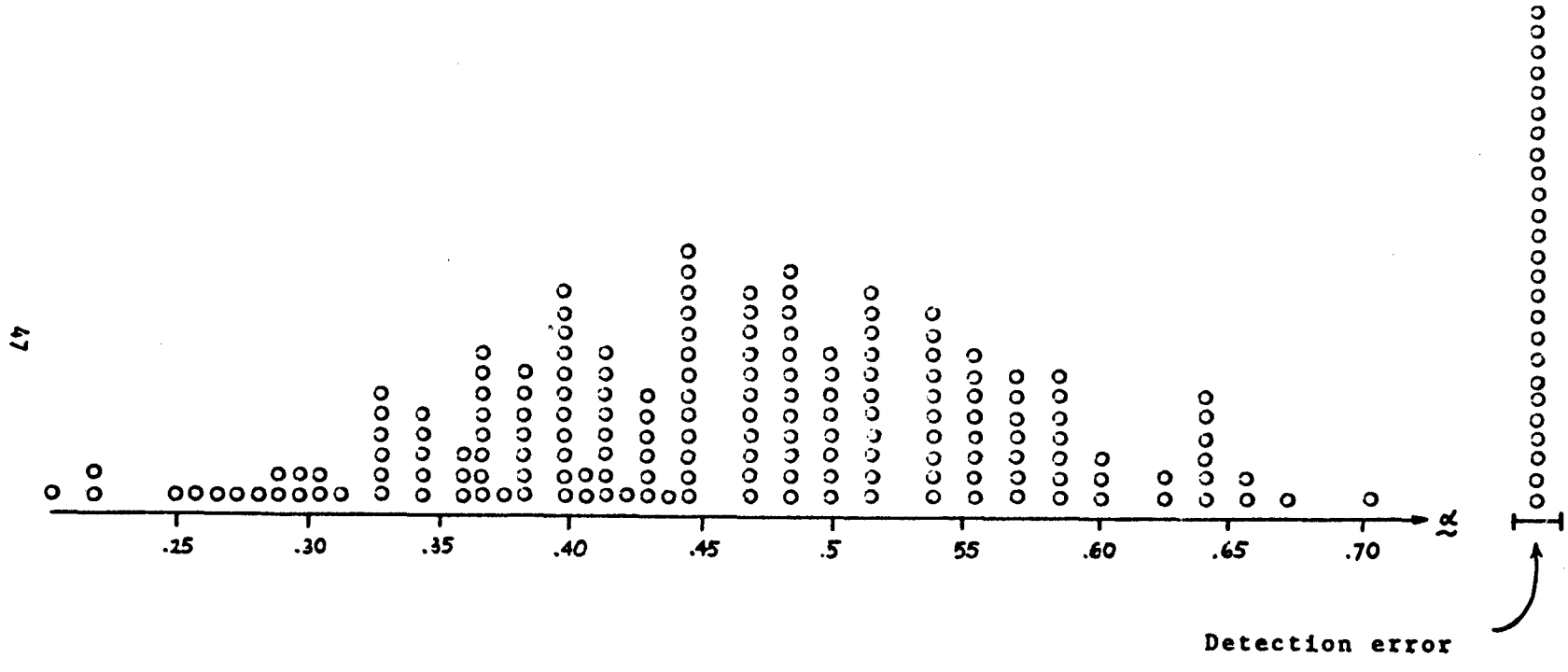

Figure C4. Multipath Detection, Codex 9600 Modem.
Estimates of α, with true $\alpha = 0.5$, $\tau \cong 2.9$ ms, $f_s = 7000$ Hz.

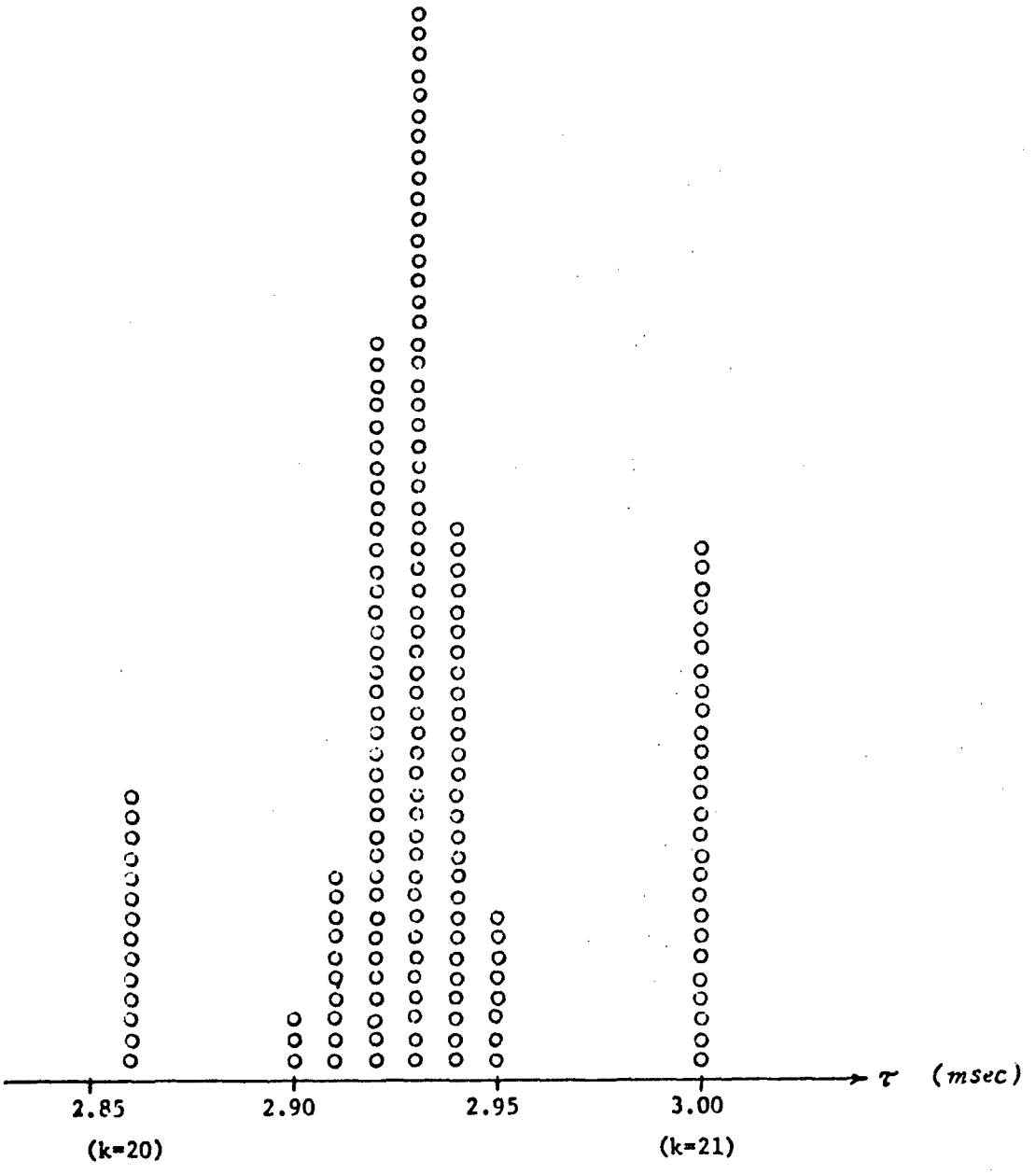

Figure C5. Multipath Detection, Codex 9600 Modem. Estimates of τ, with $\alpha = 0.5$, $f_s = 7000$ Hz. (Detection errors are not shown.)

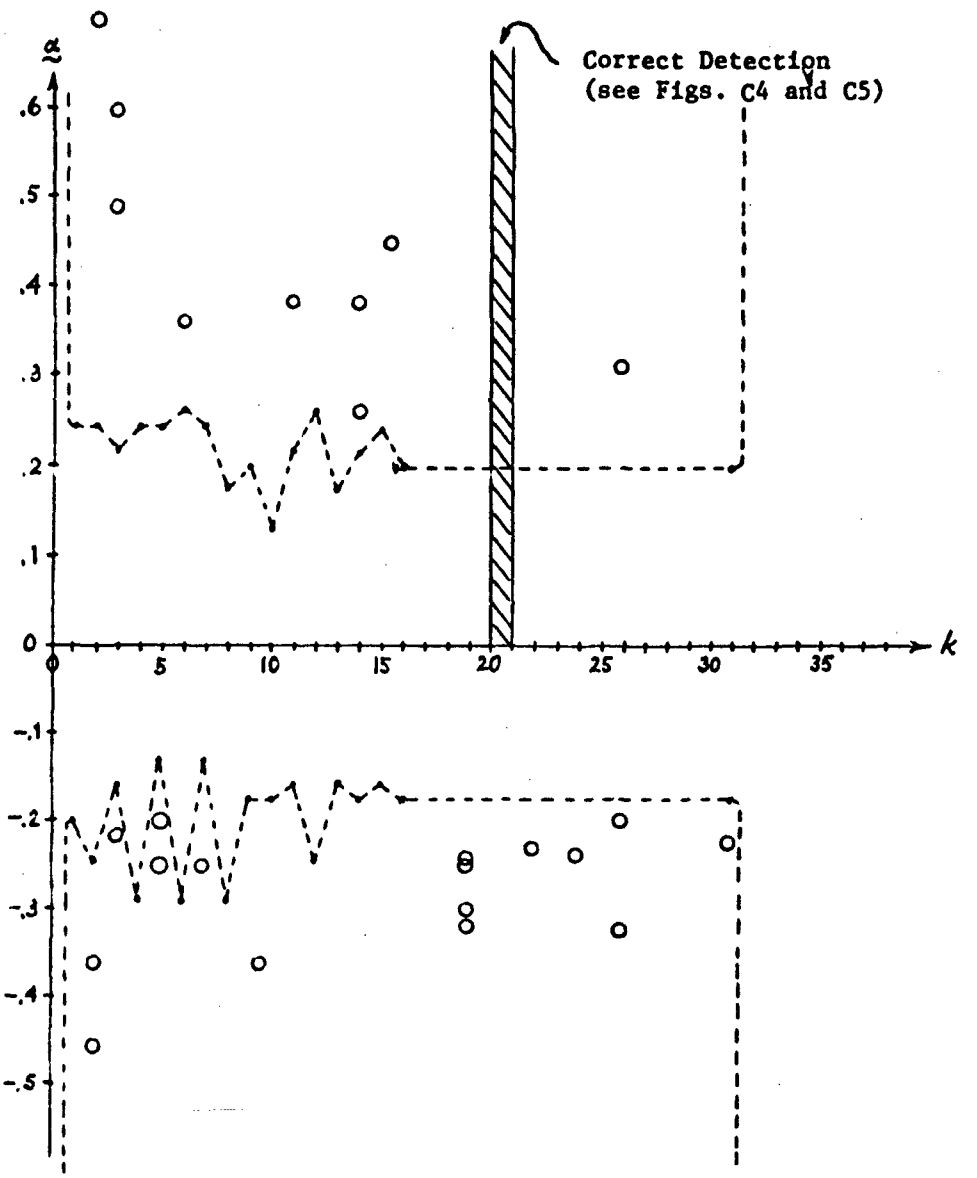

Figure C6. Multipath Detection, Codex 9600 Modem. Threshold Settings and Detection Errors with $\alpha = 0.5$, $\tau \cong 2.9$ ms; $f_s = 7000$ Hz.

2.90 to 2.95 resulted from interpolation between two adjacent cepstrum samples (#20 and #21), whereas an estimate of 2.86 (3.00) ms resulted when cepstrum sample #21 (#20) did not exceed threshold.

The detection errors are plotted in Fig. C6, together with the detection thresholds which were used. These thresholds were "hand-picked" on the basis of measured cepstrum statistics. A slightly larger negative threshold could have eliminated a few of the detection errors, but most of the errors are due to rather large random peaks which can arise in the cepstrum. Errors which occur adjacent to the location of the true multipath spike (locations 19 and 22) are in part due to the negative overshoot of the sinc-function which is associated with the multipath cepstrum.

C.3 The Hughes HC-276 Modem.

The HC-276 generates a single quadraphase PSK signal. It was operated at 2400 bits/sec. Cepstrum statistics were collected and plotted (Fig. C7) in the same manner as for the USC-9 modem. A number of detection runs performed with this modem gave similar results to those obtained with the other two modems.

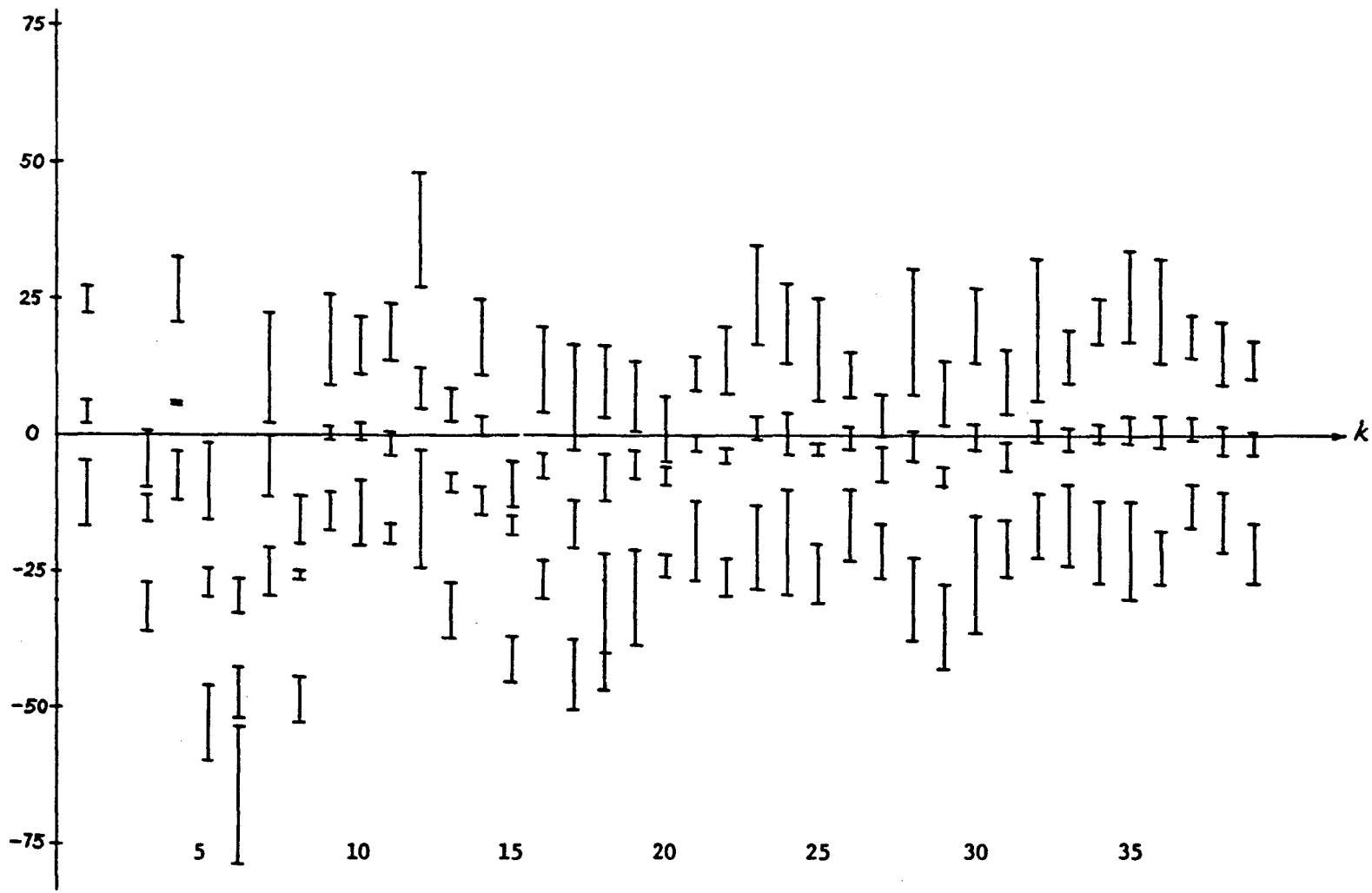

Figure C7. Hughes HC-276 Modem: Range of cepstrum maxima, minima, and mean values, for five different sets of 16 cepstra, with f_s = 7000 Hz.

APPENDIX D. ANALYSIS OF TEST DATA

D.1 Analysis of Codex 9600 Multipath Detection Data.

The Codex 9600 multipath detection test at f_s = 7000 Hz, whose results are plotted in Figs. C4, C5, and C6, is the only test in which a large number of measuremerts were performed. Nevertheless, the analysis given below is distorted by the fact that detection errors occurred, and that for each detection resulting in an error, it is not known what the α-estimate would have been in the absence of an error. In other words, the analysis is based only on those α-estimates which were associated with τ-estimates in the range from 2.86 to 3.00 ms (see Fig. C5).

Out of the 201 individual cepstrum computations, 25 led to a detection error (with the particular threshold settings used - see Fig. C6). The remaining 176 correct detections are characterized by:

	in units of cepstrum amplitude	in units of α
average value	58.7	.458
standard deviation	13.0	.102

The fact that the average value is less than the true α (α = .5, corresponding to a cepstrum amplitude of 64.0) is of no concern. The discrepancy represents the multipath cepstrum depression discussed in Section 2.4 (δ_r in Section B.7). Actually, there is another small contribution to this effect due to the fact that the interpolation is not operative unless a cepstrum sample adjacent to the maximum exceeds threshold. In Fig. C5, a detection resulting in τ = 2.86 or 3.00 ms (i.e., no interpolation) in general yields a slightly lower value of α than would be obtained if interpolation had been used without regard to threshold.

If the cepstrum values at k = 20 and k = 21 had been recorded for all the cepstra computed in this test (rather than only the cepstrum values at the position of the largest cepstrum spike), it would have been possible to include the data from those cepstra which resulted in detection errors. This presumably would have resulted in a somewhat lower average, and also a slightly larger standard deviation, since instances of low cepstrum values

at locations k = 20 and k = 21 are more likely to result in a detection error.

Based on the values in the above table, a comparison can be made with the probabilities of wrong detection computed in Sec. B.7 for the idealized Gaussian model. From the above data and Fig. C6,

$$\alpha \approx 4.5\,\sigma$$

$$\theta \approx 2\,\sigma \qquad \text{(D-1)}$$

$$D = 31$$

On the basis of the assumptions in Sec. B.7, this should give a probability of wrong detection or miss of about .02. Actually, detection errors occurred in 25 out of 201 trials, which is a relative frequency of .124. The discrepancy is mainly due to the following:

a) The cepstrum variability is not adequately characterized by a Gaussian distribution; it does not fall off as rapidly. Since the detection algorithm searches for a maximum, this is probably the most significant item.

b) The threshold settings were not carefully adjusted at every point in the cepstrum, and presumably at some locations they were less than the 2σ in (D-1).

c) Errors in the mean cepstrum estimates (see Sec. B.6) are not accounted for.

D.2 Contributions of Different Sources of Error.

The test data indicates a rather large variability of the signal cepstrum, for all three types of modems used in the tests, compared to the synthetic 16-channel PSK signal which was the basis for the earlier study reported in [1]. Since the PDP-8 routine for computing cepstrum statistics did not compile estimates of the standard deviation at each cepstrum point, an accurate comparison is not possible. A rough comparison is possible by noting:

Est. Standard deviation of 256-point 16-channel PSK signal (Figure 31 of [6]):

Approx. 5, over a large part of the detection window.

Standard deviation of multipath amplitude estimate, CODEX 9600, excluding wrong detections (Fig. C4, and Sec. D.1):

Approximately 13.

The question is now, whether the variability encountered in the test with the Codex modem is due to the nature of the signal only, or whether it is significantly influenced by the various types of errors discussed in Appendix B. In this section, the effect of the various sources of error on the variability of the cepstrum will be estimated.

a) Truncation error, on the basis of a single test (Sec. B.1), will be assumed to introduce an additive error in the cepstrum with standard deviation of .267. (The units are such that a quantization interval has size 1.0.)

b) Signal quantization superimposes an additive noise at the input. This effect will be combined with other noises appearing at the input (i.e., prior to the nonlinearity.) The quantization noise has standard deviation $1/\sqrt{12} = 0.29$.

c) Data preparation superimposes a noise on the input (see B.2) with standard deviation .35.

d) The error due to sampling jitter can be estimated from (B-1). A Codex 9600 signal sample sequence was entered at an APL terminal and the expression (B-1) computed. The signal had an r.m.s. value of 484. Application of (B-1) resulted in an error standard deviation of 9.16 at the input which clearly overshadows the errors from other sources. Taking into account the effect of data overlapping, but neglecting the effect of the window, the signal r.m.s. value becomes $484/\sqrt{2}$, and the errors in b), c), and d) combine to give

$$\sqrt{(.29/\sqrt{2})^2 + .35^2 + (9.16/\sqrt{2})^2} = 6.49 \qquad \text{(D-2)}$$

Using (F-2) as a rough means for estimating cepstrum error gives $\varepsilon_c = 2.68$. This can be combined with the truncation error of item (a) above, assuming that these errors superimpose in the cepstrum, to give

$$\sqrt{2.68^2 + .267^2} = 2.7 \qquad \text{(D-3)}$$

Using this value to correct the standard deviation of the α-estimates for the effects of errors gives

$$\sqrt{13.0^2 - 2.7^2} = 12.7 \qquad \text{(D-4)}$$

This differs very little from the uncorrected value of 13.0. However, it must be remembered that (F-2) is not directly applicable to signals from the Codex 9600 modem; it applies to the 16-channel PSK signal which Tugnait [2] used in his analysis. However, use of this formula here, without rederivation based on frequency domain statistics for the type of signal in use, can at least be expected to yield a "ball park" figure. Also the comparison in Fig. B6 of cepstrum errors computed via (F-2) and values obtained directly from different signal samples indicates that the error estimate obtained with (F-2) is low. Fig. B6 is based, of course, on data obtained with the USC-9 modem, but the cepstrum characteristics observed with all three different modem types seem roughly similar. Thus, (F-2) appears to best approximate the behavior of the less error-prone signal sequences. It can be concluded from (D-3) that sampling jitter very likely contributed noticeably to the variability in estimated multipath amplitude, whereas the effect of other sources of error is fairly insignificant.

APPENDIX E. TWO MULTIPATH COMPONENTS

E.1 The Cepstrum Due to Two Discrete Multipath Components

The computations and tests performed on this project have mostly, for simplicity, assumed that only a single multipath component is superimposed on the desired signal. At first examination it appears that the case of two (or more) multipath components is a straightforward extension of the analysis for a single multipath component, with an appropriate modification in the expansion of the logarithm ([1], equ. 2-12).

Thus, consider a received signal of the form

$$y(t) = x(t) + \alpha x(t - \tau_1) + \beta x(t - \tau_2), \tag{E-1}$$

where $x(t)$ is the transmitted, or desired, component. A sample sequence $\{y_k\}$ then has a DFT which is approximately (that is, neglecting error due to end effects or, equivalently, assuming that the signal is periodic with period T)

$$\{d_y(n)\} = \{d_x(n)(1 + \alpha e^{-j2\pi nr/N} + \beta e^{-j2\pi ns/N})\}, \tag{E-2}$$

where it is assumed for convenience that τ_1 and τ_2 are integral multiples of the sampling interval: $\tau_1 = r(T/N)$, and $\tau_2 = s(T/N)$. The logarithmic spectrum is then

$$\{\ell_y(n)\} = \{\ell_x(n)\} + \{\ell_n|1 + \alpha e^{-j2\pi nr/N} + \beta e^{-j2\pi ns/N}|\}. \tag{E-3}$$

The pattern of multipath spikes in the cepstrum arises from the last term in (E-3). Its form becomes clear upon expanding the logarithm:

$$\ell_n(1 + \alpha e^{-j2\pi nr/N} + \beta e^{-j2\pi ns/N}) = (\alpha e^{-j2\pi nr/N} + \beta e^{-j2\pi ns/N})$$

$$- \frac{1}{2}(\alpha^2 e^{-j4\pi nr/N} + 2\alpha\beta e^{-j2\pi n(r+s)/N} + \beta^2 e^{-j4\pi ns/N})$$

$$+ \ldots\ldots \tag{E-4}$$

The following cepstrum components are therefore obtained:

position	r	s	2r	r+s	2s	3r	2r+s	....
amplitude	$\frac{N\alpha}{2}$	$\frac{N\beta}{2}$	$\frac{-N\alpha^2}{4}$	$\frac{-N\alpha\beta}{2}$	$\frac{-N\beta^2}{4}$	$\frac{N\alpha^3}{6}$	$\frac{N\alpha^2\beta}{2}$	....

However, the expansion (E-4) only converges for

$$|\alpha| + |\beta| < 1, \qquad \text{(E-5)}$$

and it was first shown in [7] that the amplitudes of the cepstrum spikes have a completely different behavior, as functions of α and β, once the condition (E-5) is exceeded. In that case, the amplitude of cepstrum spikes can be obtained numerically from cepstrum computations as shown for instance in Fig. E1, which is a reproduction of Fig. 5 in [7]. Here the coefficients of significant cepstrum components have been plotted as a function of α for the case $\alpha = \beta$, with $r = 10$, $s = 17$. For $\alpha = \beta < 0.5$, the linear increase in fundamental components and quadratic increase in second-order sum components can be observed, in agreement with the above chart. A drastic change occurs in the pattern near $\alpha = \beta = 0.5$. The fundamental and second-order sum components become depressed as α and β increase further, and instead, difference components arise at $s - r = 7$, $2r - s = 3$, $2s - r = 24$, etc. The same phenomenon is also illustrated in Fig. E2, which is a plot similar to the one in Fig. E1, but for the case where β ranges from 0 to 1 while α is fixed at $\alpha = 0.8$. As β increases above 0.2, (E-5) is violated, the cepstrum spikes at r, 2r, and 3r (cepstrum points 10, 20 and 30) get depressed and the difference component at $s - r$ (=7) appears. Figures E1 and E2 show only the major cepstrum components which appear in the portion of the cepstrum that is illustrated. Additional weak components arise at higher order differences when (E-5) is violated.

E.2 Estimation of Multipath Parameters

A preliminary version of an algorithm for identifying two multipath components was developed and is presented below. A PDP-8 program implementing the algorithm has also been written, but not tested. A discussion of the algorithm follows its description.

E.2.1 Description of Algorithm

Part 1: Multipath Identification

a) Identify largest cepstrum spike which exceeds the threshold, and interpolate. Denote its interpolated peak value A_1 and its interpolated cepstrum

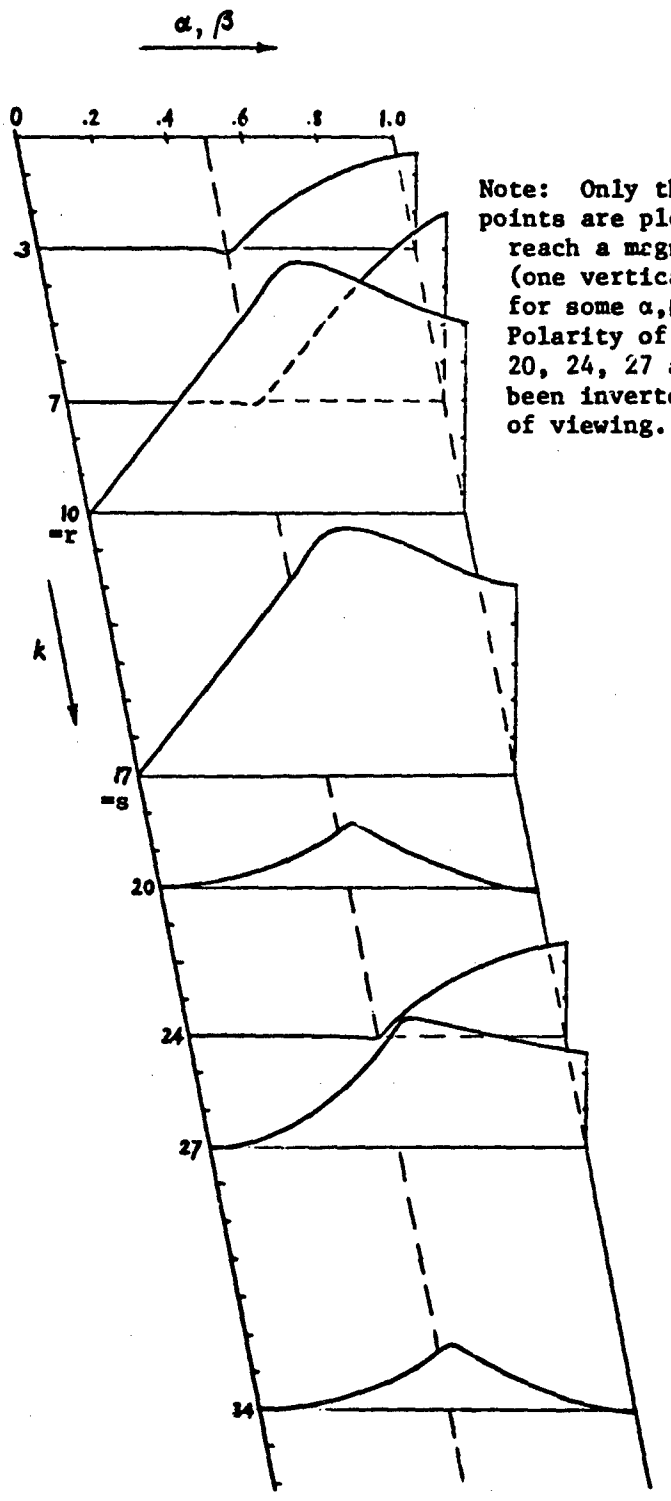

Note: Only those cepstrum points are plotted which reach a magnitude $\geq$ 10 (one vertical division) for some α,β values. Polarity of points k = 20, 24, 27 and 34 has been inverted for ease of viewing.

Figure E1. The real cepstrum for two multipath components, as function of α, with $\beta = \alpha$.

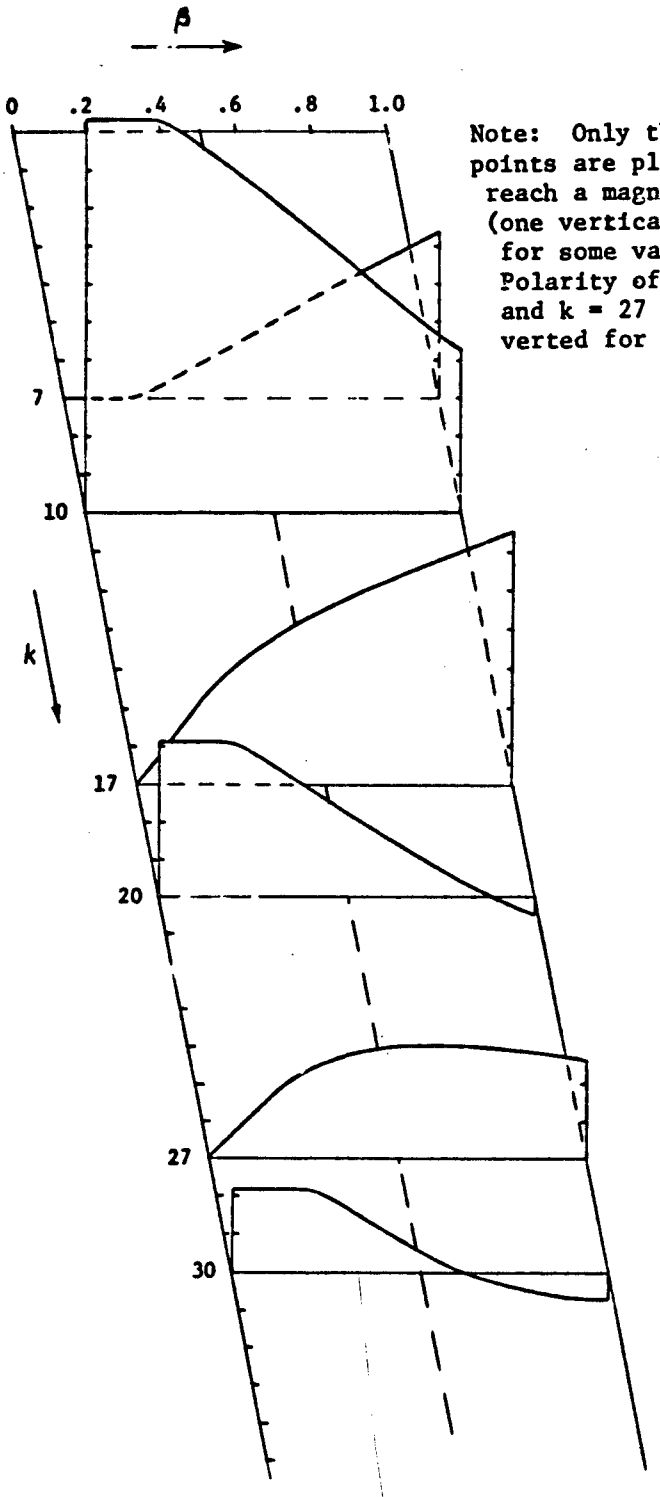

Note: Only those cepstrum points are plotted which reach a magnitude ≥ 10 (one vertical division) for some values of β. Polarity of points k = 20 and k = 27 has been inverted for ease of viewing.

Figure E2. The real cepstrum for two multipath components, as function of β, for α =0.8.

location Δ_1. If there is no point at which threshold is exceeded, the decision is "No Multipath" and the routine terminates. Otherwise, continue to step b.

b) Identify the next largest cepstrum spike which exceeds threshold, and interpolate. Denote the interpolated peak value A_2 and its interpolated cepstrum location Δ_2. If no such cepstrum spike is present, the decision is "single multipath", and the multipath parameter estimates are $\underset{\sim}{\alpha} = 2A_1/N$, $\underset{\sim}{\tau} = \Delta_1/f_s$. Otherwise, continue to step c.

c) Identify the third largest cepstrum spike which exceeds threshold, and interpolate. Denote the interpolated peak value A_3, and its interpolated cepstrum location Δ_3. If no such cepstrum spike is present, go to step g. Otherwise, continue to step d.

d) Order Δ_1, Δ_2, Δ_3 in ascending order and denote them Δ_a, Δ_b, Δ_c. (Thus, $\Delta_a \leq \Delta_b \leq \Delta_c$.) Let δ denote the time between samples. If $\Delta_a + \Delta_b = \Delta_c \pm \delta$, go to step f. Otherwise, go to step e.

e) If $\Delta_c \neq 2\Delta_b \pm \delta$, and also $\Delta_c \neq 2\Delta_a \pm \delta$, discard A_3 and Δ_3 and go to step g. Otherwise set $\tau_1 = \Delta_a$, $\tau_2 = \Delta_b$, compute the cepstrum value at $\tau_2 - \tau_1$ and go to step h.

f) If $A_1 \cdot A_2 \cdot A_3 > 0$, set $\tau_1 = \Delta_b$, $\tau_2 = \Delta_c$, take A_3 as the cepstrum value at $\tau_2 - \tau_1$, and go to step h. Otherwise, discard Δ_c and set $\tau_1 = \Delta_a$, $\tau_2 = \Delta_b$, compute the cepstrum value at $\tau_2 - \tau_1$, and go to step h.

g) Denote $\Delta_a = \max(\Delta_1, \Delta_2)$, $\Delta_b = \min(\Delta_1, \Delta_2)$. If $\Delta_b = 2\Delta_a \pm \delta/2$, and $A_b \approx -A_a^2/N$, then "single multipath" is decided, with $\underset{\sim}{\tau} = \Delta_a$, $\underset{\sim}{\alpha} = 2A_a/N$. Otherwise, continue to step h.

Part 2: Double Multipath Parameter Estimation

h) To determine whether or not (E-5) is satisfied, compute the value of the cepstrum at $\tau_2 - \tau_1$. Denote the value A_Δ. If A_Δ exceeds a preset threshold level, the decision is (E-5) is violated. In that case, go to step i; otherwise go to step j.

i) "Region I" estimates (i.e., $|\alpha| + |\beta| < 1$):

$$\underset{\sim}{\tau}_1 = \Delta_a, \quad \underset{\sim}{\tau}_2 = \Delta_b, \quad \underset{\sim}{\alpha} = 2A_a/N, \quad \underset{\sim}{\beta} = 2A_b/N$$

j) "Region II" estimates (i.e., $|\alpha| + |\beta| > 1$):

Simultaneously solve the following two equations for $\underset{\sim}{\alpha}$ and $\underset{\sim}{\beta}$:

$$44\alpha - 7.\beta = A_a - 83.5$$

$$44\beta - 77\alpha = A_b - 83.5$$

Retaining $\underset{\sim}{\alpha}/\underset{\sim}{\beta}$, scale $\underset{\sim}{\alpha}$ and $\underset{\sim}{\beta}$ to satisfy

$$\underset{\sim}{\alpha} + \underset{\sim}{\beta} = A_\Delta/57 + 1.$$

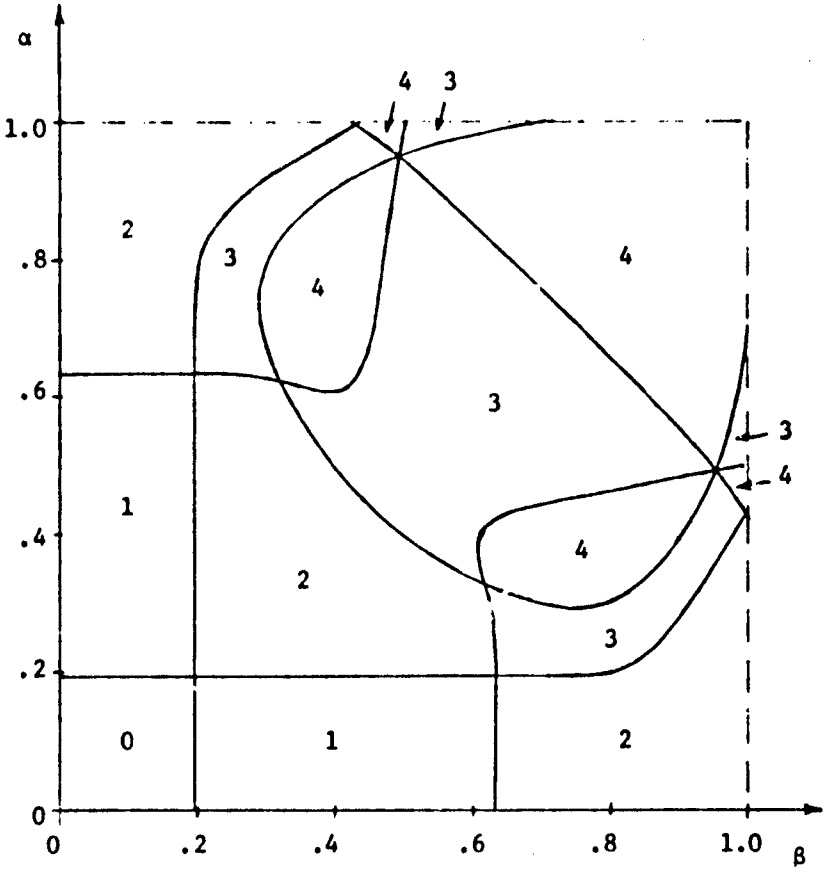

Figure E3. Number of Cepstrum Spikes which have Amplitude greater than 25, for different values of α and β. (256-point real cepstrum.)

E.2.2 Discussion of Algorithm

The algorithm presented in the preceding Section consists of two parts. The first part serves to identify the type of multipath structure which is present, and to identify the pertinent cepstrum components. The second part provides the actual parameter estimates (in the case of two multipath components).

Steps a and b are straightforward. Interpolated peak values and locations are obtained in the manner described in Sections A.2.6.1 and A.2.6.2. In step a it is decided whether or not multipath is present. In step b, if it is decided that only a single multipath component is present, the multipath parameters are estimated in the same way as in Section A.2.6.2.

In step c, a third cepstrum spike is sought which might provide additional information. If a third cepstrum spike is not found, the possibility must be considered that the two spikes which have been found are the first two spikes of a single multipath cepstrum (Fig. 1); this is done in step g.

Steps d through f apply in the case where three multipath spikes are detected. It is then necessary to decide which three they are (see Fig. E3). This problem exists even in the absence of variability due to the signal and due to additive noise, and it becomes more difficult when such variability is taken into account. In step d, if the relationship $\Delta_a + \Delta_b = \Delta_c \pm \delta$ is satisfied, it could mean either that the spikes of location Δ_a and Δ_b are the "main" multipath spikes, and Δ_c is the sum spike; or that the main spikes are at Δ_b and Δ_c, and Δ_a is the location of the first difference spike. A decision between these two possibilities is reached in step f. In step e, the possibility that the spike at Δ_c is a second harmonic component is weighed. If it is decided that this is the case, this component is discarded because it is not used in the parameter estimation procedure.

It should be noted that certain combinations which might arise have not been accounted for in this algorithm (they could be included without excessive effort), notably, the possibility of the second main spike coinciding with the harmonic of the first multipath component - i.e., the two multipath delays having a ratio of 2:1.

The second part of the algorithm requires first a decision as to whether (E-5) is satisfied ("Region I" of the α,β-plane) or not ("Region II" of the α,β-plane). Unfortunately, it is not possible to make a very sharp discrimination between the two regions, as is evident from Figs. E1 and E2. The decision is based on the value of the difference component (which ideally is zero in Region I). The Region I estimate, in step i, is straightforward since (E-4) applies.

The procedure for obtaining the Region II estimate is based on detailed plots of the multipath cepstrum amplitudes. From these, linear approximations to the empirical data were constructed which resulted in the equations in step j. The last part of step j is an attempt to improve the estimate near the boundary of Region II.

APPENDIX F. EFFECTS OF ADDITIVE NOISE

The effect in the cepstrum due to additive noise in the time domain was considered by Tugnait [2]. He proposed a simplified mathematical model for estimating the r.m.s. error in the cepstrum due to several types of additive noise, namely, impulsive noise, white Gaussian noise, and quantization noise. He compared results obtained with this model against tests performed with synthesized signal and noise sequences on APL, and found reasonably good agreement. The various types of noise which were considered have in common the property that their spectrum is uniform (in a statistical sense); and it was found that the error introduced in the cepstrum was similar for the three types of noise, for given input signal-to-noise ratio. Of course, the nature of the interference produced by additive noise depends strongly on the probability distributions governing the magnitudes $|d_x(n)|$ of the DFT of the signal sample sequences $\{x_k\}$. Tugnait used in his analysis and computations the 16-channel PSK signal, at 8175 sample/sec, which was also used in the work described in [1].

Tugnait's simplified mathematical model is obtained by partitioning the discrete frequency domain into two sets of points, one consisting of those points where $|d_x(n)|$ has a large expected value, and the other consisting of the remaining points. Within each of these two regions, the distribution of $|d_x(n)|$ is then assumed independent of n and is approximated by a mathematically simple function (triangular). After utilizing another simplifying assumption, namely that the first $\frac{N}{2}$ DFT magnitudes are characterized by mutually independent random variables, Tugnait obtains expressions from which estimates of the r.m.s. error in the cepstrum domain can be computed.

A simple empirical expression can be fitted to the error data obtained by Tugnait for the case of an interfering impulse (Fig. 4.6a and 4.6b in [2]) as follows:

$$\varepsilon_c \cong 4 \ln (1 + 32 \rho_i) \qquad \text{(F-1)}$$

where

ρ_i = ratio of r.m.s. noise to r.m.s. signal at the input (averaged over the input sequence)

ε_c = r.m.s. error per point in the cepstrum (averaged over the whole cepstrum)

Although this expression is obtained for the case of a single interfering impulse, it appears from other computations presented in [2] that white Gaussian noise produces a similar cepstrum error, for a given input noise-to-signal ratio. Therefore, (F-1) is roughly applicable for any noise with constant spectrum superimposed on a signal sequence of the type considered by Tugnait. If the noise is, in fact, a single interfering impulse, ρ_i can also be written $\sqrt{N}(S/A)$, where S is the signal r.m.s. value, A the impulse magnitude, and N the number of points being processed.

The expression (F-1) is specifically for 128-point signal sequences. However, it can be modified to apply for arbitrary N in the following manner. Consider doubling N, while keeping ρ_i constant. The signal-to-noise ratio in the DFT domain (and log spectrum) is unchanged. (If the noise is impulsive, this assumes the number of observed impulses doubles.) However, in computing the cepstrum, integration (actually summation) is now over twice as many points of the log spectrum as before, resulting in an improvement in the ratio of signal cepstrum to noise cepstrum by a factor of $\sqrt{2}$. Since the signal cepstrum increases by a factor of 2, ε_c increases only by $\sqrt{2}$. The appropriate modification of (F-1) is therefore

$$\varepsilon_c = \frac{\sqrt{N}}{2\sqrt{2}} \ln(1 + 32\,\rho_i) \qquad \text{(F-2)}$$

This equation is solved below for several different values of ρ_i with N = 256:

ρ_i	ε_c
0.0001	.0181
0.001	.178
0.01	1.57
0.1	8.1
1	19.8

APPENDIX G. SSB AND DSB SIGNALS SUBJECT TO MULTIPATH

G.1 Ordinary Synchronous Detection of SSB Signal

Suppose the baseband signal $x(t)$ is used to SSB modulate a carrier at frequency f_o. Let $\mathcal{F}_x^+(f)$ and $\mathcal{F}_x^-(f)$ denote the positive and negative frequency portions of the F.T. of $x(t)$, respectively, and $\check{x}(t)$ the Hilbert transform of $x(t)$. Assuming that the modulation resides in the upper sideband, the modulated carrier is then of the form

$$v(t) = x(t) \cos \omega_o t - \check{x}(t) \sin \omega_o t, \tag{G-1}$$

where

$$\mathcal{F}_v(f) = \mathcal{F}_x^+(f - f_o) + \mathcal{F}_x^-(f + f_o) \tag{G-2}$$

Introduction of a single, fixed, discrete multipath component of relative magnitude α and delay τ results in the distorted SSB signal

$$w(t) = v(t) + \alpha v(t - \tau) \tag{G-3}$$

whose F.T. is

$$\mathcal{F}_w(f) = \mathcal{F}_v(f) + \alpha \mathcal{F}_v(f) e^{-j2\pi f\tau}$$

$$= \mathcal{F}_x^+(f - f_o)[1 + \alpha e^{-j2\pi f\tau}] + \mathcal{F}_x^-(f + f_o)[1 + \alpha e^{-j2\pi f\tau}]. \tag{G-4}$$

Assume that the demodulator is synchronized to the phase of a reference carrier included in the SSB signal. If the received carrier phase angle in the absence of multipath is taken as 0^o, then the actual received carrier phase is

$$\theta = \arg[1 + \alpha e^{-j\omega_o\tau}] = \arctan \frac{-\alpha \sin \omega_o\tau}{1 + \alpha \cos \omega_o\tau} \tag{G-5}$$

Neglecting constant multipliers, the demodulated signal $y(t)$ is therefore given in the frequency domain by

$$\mathcal{F}_y(f) = \{\mathcal{F}_w(f) * [e^{j\theta}\delta(f - f_o) + e^{-j\theta}\delta(f + f_0)]\} H_{LP}(f)$$

$$= \{e^{j\theta} \mathcal{F}_w(f - f_o) + e^{-j\theta} \mathcal{F}_w(f + f_o)\} H_{LP}(f)$$

$$= \mathcal{F}_x^+(f)[1 + \alpha e^{-j2\pi(f+f_o)\tau}]e^{-j\theta} + \mathcal{F}_x^-(f)[1 + \alpha e^{-j2\pi(f-f_o)\tau}]e^{j\theta} \tag{G-6}$$

here $H_{LP}(f)$ is a low-pass filter function and θ is given by (G-5). ubstitution of (G-5) into (G-6) leads to

$$\mathcal{F}_y(f) = \mathcal{F}_x(f)\{[\cos\theta - j\,\mathrm{sgn}f \sin\theta] + [\alpha e^{-j2\pi f\tau}(\cos(\omega_o\tau+\theta) - j\,\mathrm{sgn}f \sin(\omega_o\tau + \theta))]\}, \quad \text{(G-7)}$$

giving

$$y(t) = x(t)\cos\theta + \check{x}(t)\sin\theta + \alpha x(t - \tau)\cos(\omega_o\tau + \theta) + \alpha\check{x}(t - \tau)\sin(\omega_o\tau + \theta). \quad \text{(G-8)}$$

This can be written

$$y(t) = [x(t) + \alpha' x(t - \tau)]\cos\theta + [\check{x}(t) - \check{x}(t - \tau)]\sin\theta, \quad \text{(G-9)}$$

where

$$\alpha' = \alpha(\cos\omega_o\tau - \sin\omega_o\tau \tan\theta) = \frac{\alpha(\alpha + \cos\omega_o\tau)}{1 + \alpha\cos\omega_o\tau}. \quad \text{(G-10)}$$

From (G-8) or (G-9) it can be seen that this type of SSB demodulation, in the presence of simple multipath at r.f., results in both in-phase and quadrature components of the baseband signal. The in-phase and quadrature delay components appear with different relative magnitudes. Also, the phase angle θ defined in (G-5) is very sensitive to small changes in τ, and so is α'. These features make cepstrum processing for multipath removal not directly applicable to the demodulated signal y(t) obtained by ordinary synchronous detection.

G.2 Complex Demodulation.

Complex demodulation of an SSB signal is achieved by means of complex sampling of the IF output, or by using both an in-phase and a quadrature carrier to perform two synchronous demodulations. With w(t) as defined in (G-3), let $\tilde{w}(t)$ denote the analytic signal corresponding to w(t). Neglecting constant multipliers, the in-phase component of the output is then

$$y_i = \mathcal{R}e[\tilde{w}(t)e^{-j2\pi f_o t}e^{-j\theta}] = w\cos(\omega_o t + \theta) + \check{w}\sin(\omega_o t + \theta). \quad \text{(G-11)}$$

Similarly, the quadrature component of the output is

$$y_q = \mathrm{Im}[\tilde{w}(t)e^{-j2\pi f_o t}e^{-j\theta}] = \tilde{w}\cos(\omega_o t + \theta) - w\sin(\omega_o t + \theta) \qquad \text{(G-12)}$$

Let $\overset{o}{y}$ denote the complex envelope of w.

$$\overset{o}{y} = y_i + jy_q = \tilde{w}e^{-j2\pi f_o t}e^{-j\theta} = \tilde{x}(t)e^{-j\theta} + \alpha\tilde{x}(t-\tau)e^{-j(\theta+\omega_o\tau)}$$

$$= [\tilde{x}(t) + \alpha'\tilde{x}(t-\tau)]e^{-j\theta}\,, \qquad \text{(G-13)}$$

where

$$\alpha' = \alpha e^{-j\omega_o\tau} \qquad \text{(G-14)}$$

Thus, the complex envelope of the complex demodulator output retains the general form of a signal disturbed by a single multipath component. However, $\overset{o}{y}$ is a complex function, so that cepstrum processing is needed for both y_i and y_q. And not only the polarity, but the phase angle associated with α' must be determined.

G.3 Synchronous Demodulation of DSB Transmission.

In the case of synchronous demodulation of DSB transmission we have, analogous to (G-1) through (G-4):

$$v(t) = x(t)\cos\omega_o t, \qquad \text{(G-15)}$$

$$\mathcal{F}_v(f) = \tfrac{1}{2}\mathcal{F}_x(f-f_o) + \tfrac{1}{2}\mathcal{F}_x(f+f_o) \qquad \text{(G-16)}$$

$$\mathcal{F}_w(f) = \mathcal{F}_v(f)[1 + \alpha e^{-j2\pi f t}] \qquad \text{(G-17)}$$

The received reference carrier phase is again given by (G-5), and we have

$$\mathcal{F}_y(f) = \left\{e^{j\theta}\mathcal{F}_w(f-f_o) + e^{-j\theta}\mathcal{F}_w(f+f_o)\right\}H_{LP}(f)$$

$$= \tfrac{1}{2}\mathcal{F}_x(f)[1 + \alpha e^{-j2\pi(f+f_o)\tau}]e^{-j\theta} + \tfrac{1}{2}\mathcal{F}_x(f)[1 + \alpha e^{-j2\pi(f-f_o)\tau}]e^{j\theta}$$

$$= \mathcal{F}_x(f)[\cos\theta + \alpha e^{-j2\pi f\tau}\cos(\theta + \omega_o\tau)]$$

$$= \mathcal{F}_x(f)\cos\theta[1 + \alpha e^{-j2\pi f\tau}(\cos\omega_o\tau + \frac{\alpha\sin^2\omega_o\tau}{1 + \alpha\cos\omega_o\tau})]$$

$$= \mathcal{F}_x(f)\cos\theta[1 + \alpha e^{-j2\pi f\tau}\frac{\cos\omega_o\tau + \alpha}{1 + \alpha\cos\omega_o\tau}] \qquad \text{(G-18)}$$

Thus, the received signal is of the form

$$y(t) = x(t) + \alpha' x(t - \tau), \tag{G-19}$$

where α' is again given by (G-10). Thus, for a given α, α' lies in the range

$$-|\alpha| \leq \alpha' \leq |\alpha|, \tag{G-20}$$

its exact value determined by $\omega_o\tau$. The coefficient cos θ in (G-18) can also be written

$$\cos\theta = \frac{1 + \alpha\cos\omega_o\tau}{\sqrt{1 + 2\alpha\cos\omega_o\tau + \alpha^2}} \tag{G-21}$$

G.4 Complex Demodulation of DSB Transmission.

With w(t) defined as the inverse transform of (G-17), let $\tilde{w}(t)$ denote the analytic signal corresponding to w(t):

$$\tilde{w}(t) = x(t)e^{j\omega_o t} + \alpha x(t-\tau)e^{j\omega_o(t-\tau)} \tag{G-22}$$

Again neglecting constant multipliers, the in-phase and quadrature components of the output are given by (G-11) and (G-12), respectively. The complex envelope of w(t) is

$$\overset{o}{y}(t) = y_i + jy_q = \tilde{w}(t)e^{-j(\omega_o t+\theta)} = [x(t) + \alpha' x(t-\tau)]e^{-j\theta}, \tag{G-23}$$

where $\alpha' = \alpha e^{-j\omega_o\tau}$, as in (G-14).

As with complex demodulation of SSB, α' is complex. However, the transmitted signal appears as the real signal in (G-23), whereas it appears in its analytic form in (G-10).

REFERENCES

1. H. Schwarzlander, "Use of the Cepstrum for Processing Multipath Signals" Technical Report RADC-TR-72-44, Rome Air Development Center, Griffiss Air Force Base, N.Y. March 1972. AD-740586.

2. J.K. Tugnait, "Effects of Additive Noise on Cepstral Analysis of Signals," Technical Report TR-73-6, Dept. of Electrical and Computer Engineering, Syracuse University, Syracuse, N.Y. June 1973.

3. W.N. Sirgany, "The Design of Signals for Effective Filtering by Cepstrum Techniques, with Application to Multipath Channels" Ph.D. Dissertation, Dept. of Electrical and Computer Engineering, Syracuse University, Syracuse, N.Y. January 1974. (To be published as RADC Technical Report).

4. R.W. Schafer, "Echo Removal by Discrete Generalized Linear Filtering" Ph.D. Dissertation, M.I.T., Cambridge, Mass , February 1968.

5. James Rothman, "FFTS-C — A Fast Fourier Transform Subroutine for Complex Data," DECUS Program Library No. 8-144. August 7, 1968.

6. C. Schenker, "The Effect of Signal Sequence Size on the Ability of a Cepstrum Signal Processor to Detect Multipath" M.S. Thesis, Syracuse University, May 1972.

7. H. Schwarzlander, "A Cepstrum Processor for Signals with Multipath Distortion," Signal Processing Conference, Erlangen, Germany, April 4-6, 1973.

8. W. Sirgany, "Signal Design for Improved Multipath Identification in the Cepstrum" Tech. Memo. TM-73-2, Department of Electrical and Computer Engineering, Syracuse University, Syracuse, N.Y. June 1973.

MISSION
of
Rome Air Development Cente.

RADC is the principal AFSC organization charged with planning and executing the USAF exploratory and advanced development programs for information sciences, intelligence, command, control and communications technology, products and services oriented to the needs of the USAF. Primary RADC mission areas are communications, electromagnetic guidance and control, surveillance of ground and aerospace objects, intelligence data collection and handling, information system technology, and electronic reliability, maintainability and compatibility. RADC has mission responsibility as assigned by AFSC for demonstration and acquisition of selected subsystems and systems in the intelligence, mapping, charting, command, control and communications areas.